Published in Journal of the American Chemical Society (JACS) 120, issue 47, pp. 12274–12288, 1998,
which should be used for any reference to this work

Bent Tridentate Receptors in Calamitic Mesophases with Predetermined Photophysical Properties: New Luminescent Lanthanide-Containing Materials

Homayoun Nozary,[†] Claude Piguet,*[,†] Paul Tissot,[†] Gérald Bernardinelli,[§] Jean-Claude G. Bünzli,[‡] Robert Deschenaux,[⊥] and Daniel Guillon[||]

Contribution from the Department of Inorganic, Analytical and Applied Chemistry, Université de Genève, 30 quai E. Ansermet, CH-1211 Geneva 4, Switzerland, Laboratory of X-ray Crystallography, Université de Genève, 24 quai E. Ansermet, CH-1211 Geneva 4, Switzerland, Institute of Inorganic and Analytical Chemistry, Université de Lausanne, BCH 1402, CH-1015 Lausanne, Switzerland, Institut de Chimie, Université de Neuchâtel, 51 Avenue de Bellevaux, CH-2000 Neuchâtel, Switzerland, and Groupe des Matériaux Organiques, Institut de Physique et de Chimie des Matériaux de Strasbourg, 23 rue du Loess, F-67037 Strasbourg Cedex, France

Abstract: A new synthetic strategy has been developed to introduce bent and rigid tridentate 2,6-bis-(benzimidazol-2′-yl)pyridine cores into rodlike ligands L^{11-17}. The crystal structure of the nonmesogenic ligand L^{13} ($C_{39}H_{37}N_5O_4$, triclinic, $P\bar{1}$, $Z = 2$) shows the expected *trans*−*trans* conformation of the tridentate binding unit, which provides a linear arrangement of the semirigid aromatic sidearms. The crystal structure of the related mesogenic ligand L^{16} ($C_{61}H_{81}N_5O_4$, triclinic, $P\bar{1}$, $Z = 2$) demonstrates the fully extended conformation adopted by the lipophilic side chains, leading to a slightly helically twisted I-shaped molecule. A rich and varied mesomorphism results which can be combined with the simultaneous tuning of electronic and photophysical properties via a judicious choice of the spacers between the rigid central core and the semirigid lipophilic sidearms. Ligands $L^{13,14}$ react with $Ln(NO_3)_3 \cdot xH_2O$ to give quantitatively and selectively the neutral 1:1 complexes $[Ln(L^i)(NO_3)_3]$ (Ln = La to Lu), which are stable in the solid state at room temperature but partially dissociate in acetonitrile to give the cationic species $[Ln(L^i)(NO_3)_2]^+$. The crystal structure of $[Lu\text{-}(L^{13})(NO_3)_3] \cdot 3CH_3CN$ (**30**, $LuC_{45}H_{46}N_{11}O_{13}$, monoclinic, $C2/c$, $Z = 8$) reveals a U-shaped arrangement of the ligand strand arising from the *cis*−*cis* conformation of the coordinated tridentate binding unit. This drastic geometric change strongly affects the thermal behavior and the photophysical and electronic properties of the lipophilic complexes $[Ln(L^{14})(NO_3)_3]$. Particular attention has been focused on structure−properties relationships, which can be modulated by the size of the lanthanide metal ions.

Introduction

The recent recognition of the importance of metallomesogens (i.e., liquid crystals containing metal ions) for the development of advanced materials[1] with new electronic, optical, and magnetic properties[2] has encouraged coordination chemists to design new lipophilic rodlike or disklike complexes exhibiting mesomorphic behavior.[3] Liquid crystalline (or mesomorphic) properties result from phases in which the molecular order is intermediate between that of an ordered solid crystal and a disordered liquid. A thermotropic mesophase is formed by the influence of temperature, and the resulting thermotropic liquid crystals are divided in two main categories depending on their molecular axial anisotropies: calamitic (rodlike) and discotic (disklike).[3] A large variety of bidentate chelating units has been successfully used for the design of metallomesogens,[3] but it has been shown that metal complexes with thermotropic calamitic[5] and discotic[6] mesogenic ligands containing linear bidentate 2,2′-bipyridine units[4] display only poor[7] or no[8] mesogenic behavior. The origin of these failures has been tentatively attributed (i) to the large increase of the electric dipole moment which occurs upon complexation[8] and (ii) to the limited anisometry of the rigid core, although this has been recently overcome in extended systems.[9] The closely related tridentate receptor 2,2′:6′,2″-terpyridine is essentially ignored in this field,[3] as are other tridentate binding units.[10] To the best of our knowledge, a single

* To whom correspondence should be addressed. E-mail: Claude.Piguet@chiam.unige.ch.
[†] Department of Inorganic, Analytical and Applied Chemistry, Université de Genève.
[§] Laboratory of X-ray Crystallography, Université de Genève.
[‡] Institute of Inorganic and Analytical Chemistry, Université de Lausanne.
[⊥] Institut de Chimie, Université de Neuchâtel.
[||] Institut de Physique et de Chimie des Matériaux de Strasbourg.

(1) Giroud-Godquin, A. M.; Maitlis, P. M. *Angew. Chem., Int. Ed. Engl.* **1991**, *30*, 375. Hudson, S. A.; Maitlis, P. M. *Chem. Rev.* **1993**, *93*, 861.
(2) Bruce, D. W. *J. Chem. Soc., Dalton Trans.* **1993**, 2983.
(3) *Metallomesogens, Synthesis, Properties and Applications*; Serrano, J. L., Ed.; VCH: Weinheim, 1996.
(4) Summers, L. A. *Adv. Heterocycl. Chem.* **1984**, 281. Constable, E. C. *Adv. Inorg. Chem. Radiochem.* **1989**, *34*, 1.
(5) El-Ghayoury, A.; Douce, L.; Ziessel, R.; Seghrouchni, R.; Skoulios, A. *Liq. Cryst.* **1996**, *21*, 143. Douce, L.; Ziessel, R.; Seghrouchni, R.; Skoulios, A.; Campillos, E.; Deschenaux, R. *Liq. Cryst.* **1996**, *20*, 235. Bruce, D. W.; Rowe, K. E. *Liq. Cryst.* **1995**, *18*, 161.
(6) Palmans, A. R. A.; Vekemans, J. A. J. M.; Fischer, H.; Hickmet, R. A.; Meijer, E.-W. *Chem. Eur. J.* **1997**, *3*, 300.
(7) Kuboki, T.; Araki, K.; Yamada, M.; Shiraishi, S. *Bull. Chem. Soc. Jpn.* **1994**, *67*, 948.
(8) Rowe, K. E.; Bruce, D. W. *Liq. Cryst.* **1996**, *20*, 183.
(9) Rowe, K. E.; Bruce, D. W. *J. Chem. Soc., Dalton Trans.* **1996**, 3913. Morrone, S.; Guillon, D.; Bruce, D. W. *Inorg. Chem.* **1996**, *35*, 7041.
(10) Serrete, A. G.; Swager, T. M. *Angew. Chem., Int. Ed. Engl.* **1994**, *33*, 2342. Lai, C. K.; Serrette, A. G.; Swager, T. M. *J. Am. Chem. Soc.* **1992**, *114*, 7949. Serrette, A. G.; Lai, C. K.; Swager, T. M. *Chem. Mater.* **1994**, *6*, 2252.

Chart 1

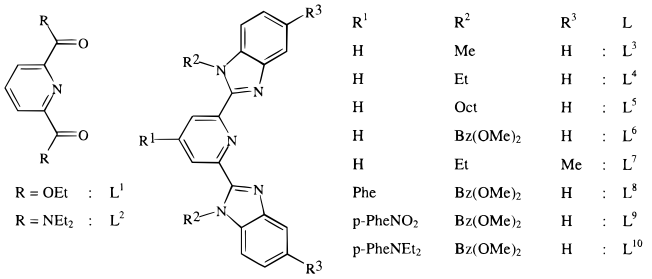

R^1	R^2	R^3		L
H	Me	H	:	L^3
H	Et	H	:	L^4
H	Oct	H	:	L^5
H	$Bz(OMe)_2$	H	:	L^6
H	Et	Me	:	L^7
Phe	$Bz(OMe)_2$	H	:	L^8
p-$PheNO_2$	$Bz(OMe)_2$	H	:	L^9
p-$PheNEt_2$	$Bz(OMe)_2$	H	:	L^{10}

example of lyotropic mesophases with Ru(II)[11] coordinated to terminal 4′-substituted terpyridine derivatives has been reported, and the analogous 4′-substituted tridentate C,N,N chelating ligand 6-phenyl-2,2′-bipyridine cyclometalated to Pd(II) displays a monotropic nematic phase at high temperature.[12] We have shown[13] that related tridentate ligands L^{1-10} (Chart 1) are particularly well-suited to produce lanthanide building blocks $[Ln(L^i)(NO_3)_3]$ ($i = 3-10$)[14] and $[Ln(L^i)_3](ClO_4)_3$ ($i = 1-10$),[15] exhibiting predetermined structural, thermodynamic, magnetic, and spectroscopic characteristics which might induce fascinating new properties in advanced materials. The recent incorporation of related lanthanide complexes into Langmuir−Blodgett films to produce luminescent materials[16] and into magnetically adjustable liquid crystals[17] demonstrates the potential of this approach. However, the inherent bent conformations associated with either free (*trans*−*trans*) or complexed (*cis*−*cis*) chelating tridentate aromatic binding units severely limits the design of rodlike or disklike molecules required for the formation of calamitic or discotic mesophases, respectively.[1−3,10] The relative weakness of the Ln−N(heterocyclic) bond[15,18] together with the ionic size[8,9] and high coordination number of Ln(III) are also crucial factors which must be considered if these building blocks are to be introduced into thermotropic mesophases.[19]

In this paper, we present a new approach aimed at introducing bent rigid tridentate aromatic receptors related to L^{3-10} into extended rodlike molecules suitable for the preparation of calamitic mesophases. Substitution of the lateral benzimidazole rings at the 4- or 5-positions is promising because the conformational change occurring upon complexation to Ln(III) (*trans*−*trans* → *cis*−*cis*, Figure 1) interconverts the topological orientation of these substituents.[14,20] However, the need for large molecular anisometry combined with suitable intermolecular interactions to produce calamitic mesophases (five aromatic rings are required for metallomesogens based on 2,2′-bipyridine units)[9] has led us to connect lipophilic tails with additional rigid aromatic groups to the 5-positions of the benzimidazole rings. Structural and electronic changes resulting from the complexation process are crucial points which have been carefully investigated in order to establish structure−function relationships. A partial report of this work appeared as a preliminary communication.[21]

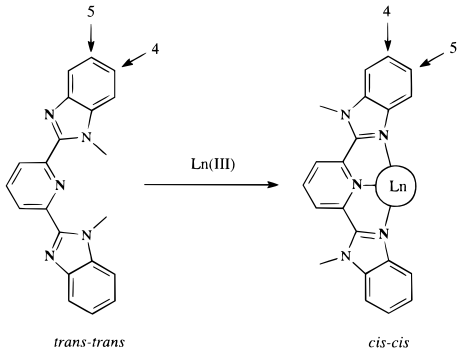

Figure 1. Conformational changes occurring upon complexation of L^3 to Ln(III).

Results and Discussion

Synthesis of the Ligands L^{11-17}. We have developed a convergent synthetic approach leading to the preparation of two different tridentate binding units substituted at the 5-positions of the benzimidazole rings with carbon (**8**) or oxygen linkers (**9,** Scheme 1). Tunable semirigid *para*-disubstituted phenyl rings bearing long terminal lipophilic alkyloxy chains (**14**, **16**−**21**, Scheme 2) can be then easily attached to the central core using modulable three- ($L^{11,12}$) or two-atom (L^{13-17}) spacers (Scheme 3). The synthons **8** and **9** are synthesized by using a recently developed strategy based on a modified Phillips reaction,[22] in which the two benzimidazole rings are formed in one step from the symmetrical bis-*o*-nitroarenecarboxamides **6** and **7**. Surprisingly, the treatment of **8** with boron tribromide followed by hydrolysis produces quantitatively the bis-bromomethyl derivative **10** instead of the expected bis-hydroxymethyl compound as a result of the high sensitivity of the benzylic positions toward nucleophilic displacements. Subsequent nucleophilic attacks with carboxylate (**14**, **19**) or phenolate (**16**−**18**) groups provide the ligands L^{11-15} in good yields. A similar deprotection procedure for **9** gives the expected and poorly soluble bis-hydroxy compound **11**, which is transformed into ligands $L^{16,17}$ by electrophilic attack of its deprotonated salt $(NBu_4)_2$[**11**-2H] with **21** or the acyl chloride derivative of **19**, respectively. The ^1H and ^{13}C NMR spectra of L^{11-17} confirm the proposed structures, and the systematic absence of observable NOE effects between the protons of the ethyl substituents of the benzimidazole ring ($H^{8,9}$) and the pyridine proton H^2 strongly suggests a *trans*−*trans* conformation (i.e., the nitrogen of the pyridine ring is *trans* to the unsubstituted nitrogen atoms of the benzimidazole rings)[14] of the tridentate binding unit in

(11) Holbrey, J. D.; Tiddy, G. J. T.; Bruce, D. W. *J. Chem. Soc., Dalton Trans.* **1995**, 1769.
(12) Neve, F.; Ghedini, M.; Crispini, A. *Chem. Commun.* **1996**, 2463. Neve, F.; Ghedini, M.; Francescangeli, O.; Campagna, S. *Liq. Cryst.* **1998**, *24*, 673.
(13) For reviews, see: Piguet, C. *Chimia* **1996**, *50*, 144. Piguet, C.; Bünzli, J.-C. G. *Eur. J. Solid State Inorg. Chem.* **1996**, *33*, 165. Piguet, C.; Bünzli, J.-C. G. *Chimia* **1998**, *52*, 579.
(14) Piguet, C.; Williams, A. F.; Bernardinelli, G.; Moret, E.; Bünzli, J.-C. G. *Helv. Chim. Acta* **1992**, *75*, 1697. Petoud, S.; Bünzli, J.-C. G.; Schenk, K. J.; Piguet, C. *Inorg. Chem.* **1997**, *36*, 1345.
(15) Piguet, C.; Williams, A. F.; Bernardinelli, G.; Bünzli, J.-C. G. *Inorg. Chem.* **1993**, *32*, 4139. Piguet, C.; Bünzli, J.-C. G.; Bernardinelli, G.; Bochet, C. G.; Froidevaux, P. *J. Chem. Soc., Dalton Trans.* **1995**, 83. Petoud, S.; Bünzli, J.-C. G.; Renaud, F.; Piguet, C.; Schenk, K. J.; Hopfgartner, G. *Inorg. Chem.* **1997**, *36*, 5750.
(16) Qian, D.-J.; Yang, K.-Z.; Nakahara, H.; Fukuda, K. *Langmuir* **1997**, *13*, 5925.
(17) Wang, Z. K.; Huang, C. H.; Zhou, F. Q. *Solid State Commun.* **1995**, *95*, 223. Galymetdinov, Y.; Athanassopoulou, A. M.; Kharitonova, O.; Soto-Bustamante, E. A.; Ovchinnikov I. K.; Hasse, W. *Chem. Mater.* **1996**, *8*, 922. Bikhantaev, I.; Galymetdinov, Y.; Kharitonova, O.; Ovchinnikov, I. K.; Bruce, D. W.; Dunmur, D. A.; Guillon, D.; Heinrich, B. *Liq. Cryst.* **1996**, *20*, 489.
(18) Forsberg, J. H. *Coord. Chem. Rev.* **1973**, *10*, 195.
(19) Pegenau, A.; Göring, P.; Tschierske, C. *Chem. Commun.* **1996**, 2563. Deschenaux, R.; Goodby, J. W. In *Ferrocenes;* Togni, A., Hayashi, T., Eds.; VCH: Weinheim, 1995; p 471ff.
(20) Piguet, C.; Rivara-Minten, E.; Hopfgartner, G.; Bünzli, J.-C. G. *Helv. Chim. Acta* **1995**, *78*, 1541.
(21) Nozary, H.; Piguet, C.; Tissot, P.; Bernardinelli, G.; Deschenaux, R.; Vilches, M.-T. *Chem. Commun.* **1997**, 2101.
(22) Piguet, C.; Bocquet, B.; Hopfgartner, G. *Helv. Chim. Acta* **1994**, *77*, 931.

Scheme 1[a]

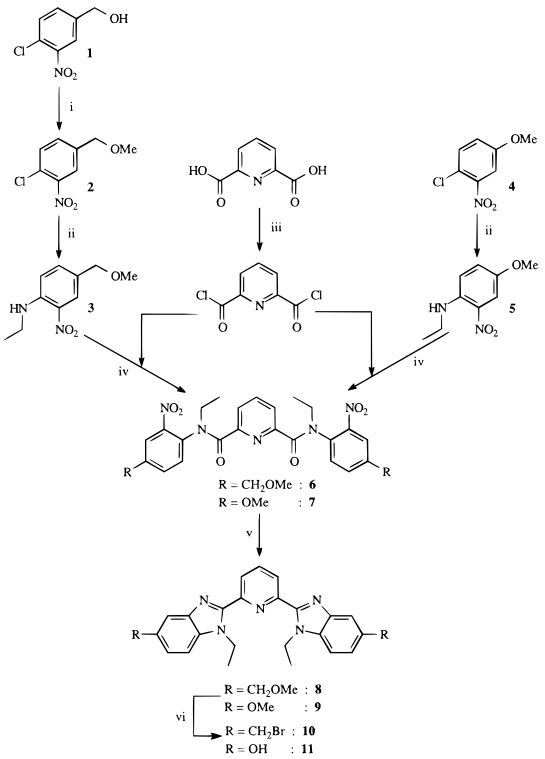

[a] Reagents: (i) KOH, DMSO, MeI; (ii) $EtNH_2$, EtOH; (iii) $SOCl_2$, CH_2Cl_2, $DMF_{cat.}$; (iv) NEt_3, CH_2Cl_2; (v) Fe, HCl, EtOH, H_2O; (vi) BBr_3, CH_2Cl_2.

Scheme 2[a]

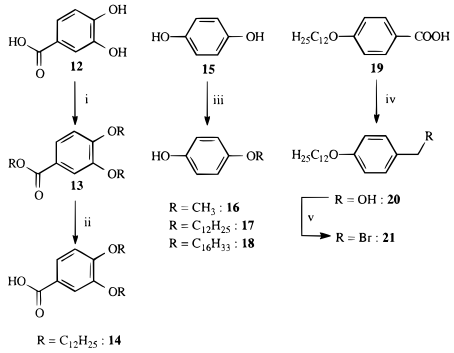

[a] Reagents: (i) $C_{12}H_{25}Br$, KOH, DMSO; (ii) KOH, EtOH, H_2O; (iii) RBr, $KHCO_3$, dioxane−water; (iv) $LiAlH_4$, THF; (v) PBr_3, CH_2Cl_2.

solution, as previously proposed for terpyridine derivatives.[23] A related *trans*−*trans* arrangement is observed in the crystal structure of the protonated ligand $[L^3 + H](ClO_4)$,[14] but a complete structural and geometrical characterization of the free unprotonated ligands is required since this point is crucial for the development of rodlike molecules incorporating bent tridentate units.

Crystal Structures of L^{13} and L^{16}. Figure 2 shows the atomic numbering scheme for L^{13} and L^{16}, and Figures 3 and 4 display ORTEP[24] stereoviews of the ligands. Atomic coordinates, displacement parameters, bond distances, bond angles, and least-squares plane data are given as Supporting Information (Tables S1−S8).

(23) Bessel, C. A.; See, R. F.; Jameson, D. L.; Churchill, M. R.; Takeuchi, K. J. *J. Chem. Soc., Dalton Trans.* **1992**, 3223 and references therein. Constable, E. C.; Lewis, J.; Liptrot, C. M. *Inorg. Chim. Acta* **1990**, *178*, 47.

(24) Johnson, C. K. *Ortep II*; Report ORNL-5138; Oak Ridge National Laboratory: Oak Ridge, TN, 1976.

Scheme 3[a]

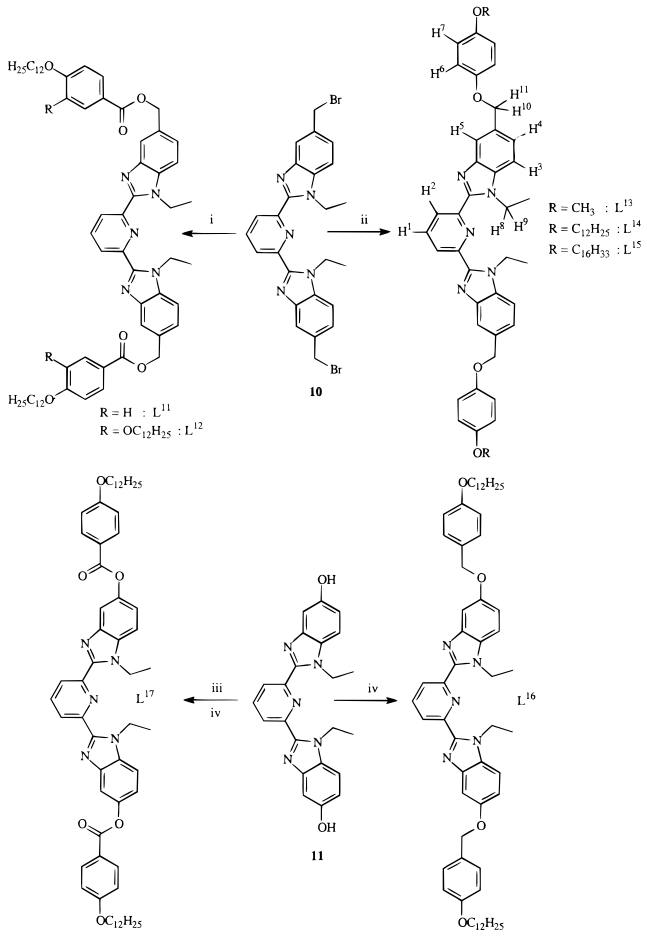

[a] Reagents: (i) **14** or **19**, NBu_4OH, CH_2Cl_2; (ii) **16**−**18**, NBu_4OH, CH_2Cl_2; (iii) **19**, $SOCl_2$, CH_2Cl_2, $DMF_{cat.}$; (iv) **21**, NBu_4OH, CH_2Cl_2.

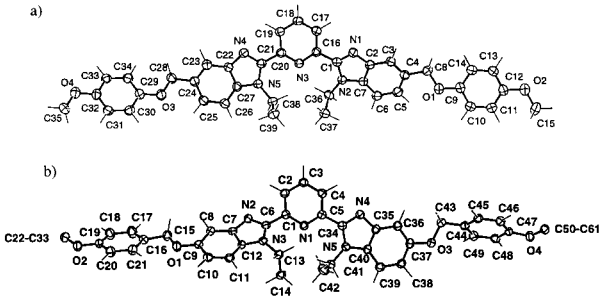

Figure 2. Atomic numbering scheme for (a) L^{13} and (b) $L.^{16}$ Ellipsoids are represented at 50% probability level.

The central aromatic cores of L^{13} and L^{16} are very similar, except for the inversion of the carbon and oxygen atoms of the spacer between the benzimidazole rings and the *para*-disubstituted phenyl sidearms. C−C, C−O, and C−N bond distances and bond angles are within standard values[26] for both ligands. The dihedral angles involving the carbon and oxygen atoms of the spacers as the central atoms (C8−O1 and C28−O3 for L^{13}, C15−O1 and C43−O3 for L^{16}) are close to 180° (174.5−179.7°), leading to an elongated antiperiplanar arrangement of the benzimidazole and phenyl rings. The tridentate 2,6-bis(benzimidazol-2-yl)pyridine units adopt the expected *trans*−*trans* conformation, which minimizes the dipolar moment and the repulsion between nitrogen lone pairs[26] and maximizes

(25) Allen, F. H.; Kennard, O.; Watson, D. G.; Brammer, L.; Orpen, A. G.; Taylor, R. *J. Chem. Soc., Perkin Trans. 2* **1987**, S1.

(26) Case, F. H.; Kasper, T. J. *J. Am. Chem. Soc.* **1956**, *78*, 5842.

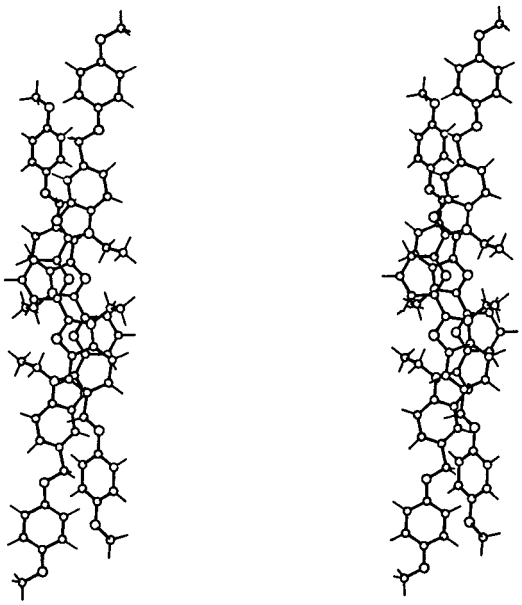

Figure 3. ORTEP[24] stereoview of a stacked pair of ligands L^{13}.

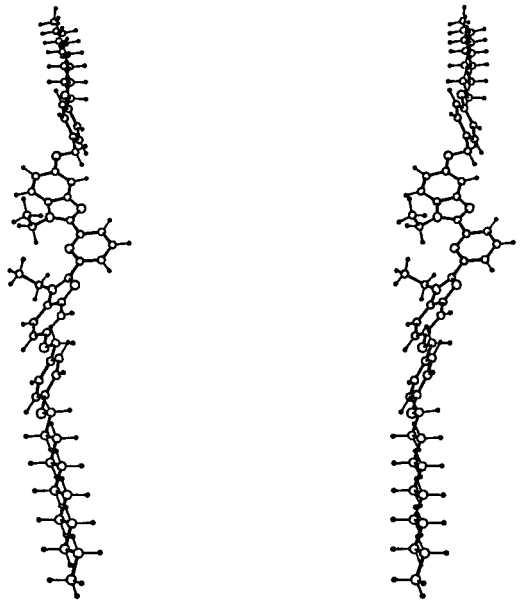

Figure 4. ORTEP[24] stereoview of L^{16}, showing the helical twist of the aromatic core.

π-overlap as established for terpyridine derivatives.[12] However, deviation from planarity is significant for both ligands, with dihedral interplanar angles between the central pyridine and the connected benzimidazole rings in the range 3−36° (Tables S4 and S8). The lateral *para*-disubstituted phenyl rings also display sizable interplanar angles with the benzimidazole rings to which they are connected via the two-atom spacer (22−61°), leading to a wavy arrangement of the five aromatic rings in L^{13} (Figure 3) and a helical twist in L^{16} resulting from a sequence of interannular rotations between the aromatic rings with the same screw direction (Figure 4). The total length between the terminal oxygen atoms of the semirigid cores (O2···O4) is similar for both ligands (29.07 Å for L^{13} and 28.63 Å for L^{16}), thus producing elongated (I-shape) basic units. As a result of the *trans*−*trans* conformation of the tridentate binding units, the *all-trans* terminal lipophilic dodecyloxy chains in L^{16} are approximately collinear and run in opposite directions, giving a highly anisotropic rodlike ligand with a total length of ca. 58.0 Å (C33···C61), a width of ca. 5.8 Å (C3···C42), and a length/width ratio of 10. In L^{13}, the almost coplanar pyridine−benzimidazole unit (interplanar angle 3.2°) of one ligand strongly interacts with the related unit of a second molecule related by an inversion center, producing head-to-tail π-stacked pairs in the unit cell aligned with their long molecular axis, making an angle of 13° with the [1 $\bar{1}$ 1] direction (Figure 3). The slight helical twist observed for L^{16} (the total helical torsion angle of the rigid core amounts to ≈136° for a total length of ≈28.6 Å, thus leading to an approximate pitch of 76 Å) prevents strong interstrand stacking interactions, and the elongated ligands are packed in the unit cell with their long molecular axis aligned in a common direction, making angles of 51°, 70°, and 62° with *a*, *b*, and *c*, respectively (Figure 4).

Mesogenic Properties of Ligands L^{11-17}. The mesomorphic properties of the ligands have been investigated by a combination of differential scanning calorimetry (DSC), polarized optical microscopy, and X-ray diffraction. $L^{11,12}$ possess three-atom spacers (CH_2−O−CO) between the benzimidazole rings and the *para*-disubstituted phenyl rings and do not exhibit mesogenic behavior. The crystals melt to give the isotropic fluids (Table 1). Attachment of a second dodecyloxy chain in L^{12} does not induce mesomorphism but decreases the melting point by 18 °C. The use of two-atom spacers in L^{13-17} severely decreases the degrees of freedom of the aromatic core, as demonstrated by the rodlike shape adopted by L^{13} in the solid state. The crystal phase in L^{13} is stable, and the melting process leads only to isotropization at high temperature. The connection of two peripheral lipophilic chains in $L^{14,15}$ induces the formation of an enantiotropic smectic A (S_A) phase and a monotropic smectic C (S_C) one. X-ray diffraction studies at small angles for L^{14} in the S_A phase at 150 °C gives a *d*-layer spacing of 51 Å (Figure F2, Supporting Information). Compared to the total length found for the closely related ligand L^{16} in its fully extended conformation in the solid state (l = 58.0 Å), we calculate a *d*/*l* ratio of 0.88, which is compatible with monomolecular organization with a pronounced disorganization of the chains.

L^{16} is similar to L^{14} except for the inversion of the carbon and oxygen atoms of the spacers, but this has only little effect on the mesomorphic behavior. On the other hand, the replacement of the CH_2 unit of the spacer with a carbonyl group in L^{17} produces different mesogenic properties with the formation of enantiotropic S_C, S_A, and nematic phases. According to the unpredictable effects of carbonyl groups on mesomorphic and ferroelectric properties of liquid crystals containing extended heterocyclic cores,[3,8,27] this peculiar behavior is not completely unexpected, but the poor resistance of aromatic esters toward hydrolysis strongly limits their use as ligands for lanthanide metal ions.

Photophysical Properties of Ligands L^{13-17}. Except for better resolution in solution, the absorption spectra of the ligands L^{13-17} are similar for solid-state (reflectance spectra) and solution (transmission spectra) samples, which suggests that the *trans*−*trans* conformation of the tridentate binding unit exemplified in the crystal structures of L^{13} and L^{16} is maintained in solution, in agreement with NMR data. A previous spectroscopic study showed the electronic absorption spectrum of L^7 in solution to be dominated by an intense transition with a maximum at 30 860 cm^{-1}, assigned to the $\pi_1(A_2) \rightarrow \pi^*(B_1)$ transition centered on the tridentate binding unit (*trans*−*trans* conformation, C_{2v} symmetry), and shoulders at higher energies involving low-lying π orbitals.[15] It was suggested that π-donor

(27) Hoschino, N.; Takahashi, K.; Sekiuchi, T.; Tanaka, H.; Matsunaga, Y. *Inorg. Chem.* **1998**, *37*, 882.

Table 1. Phase-Transition Temperatures and Enthalpy and Entropy Changes for Ligands L^{11-17} and Thermal Behavior of the Complexes $[Ln(L^{14})(NO_3)_3]\cdot xH_2O$ (**22**−**29**)

compound	transition[a]	*T*/°C	Δ*H*/kJ·mol^{-1}	Δ*S*/J·mol^{-1}·K^{-1}
L^{11}	K−I	107	80	211
L^{12}	K−I	89	112	309
L^{13}	K−I	195	46	99
L^{14}	K−S_A	132	50	122
	(S_C−S_A)[b]	98[f]	*c*	
	S_A−I	188	17	37
L^{15}	K−S_A	130	57	141
	(S_C−S_A)[b]	105	*c*	
	S_A−I	184	19	40
L^{16}	K−S_A	144	28	66
	(S_C−S_A)[b]	107[f]	*c*	
	S_A−I	193	18	39
L^{17}	K−S_C	131	35	86
	S_C−S_A	217	*c*	
	S_A−N	223	*d*	
	N−I	226	7[e]	14[e]
$[La(L^{14})(NO_3)_3]\cdot 3H_2O$ (**22**)	loss: 2 H_2O	25−80		
	loss: 1 H_2O	100−125		
	dec[g]	130		
$[Sm(L^{14})(NO_3)_3]\cdot H_2O$ (**23**)	loss: 1 H_2O	25−110		
	dec[g]	132		
$[Eu(L^{14})(NO_3)_3]\cdot H_2O$ (**24**)	loss: 1 H_2O	25−100		
	dec[g]	132		
$[Gd(L^{14})(NO_3)_3]\cdot H_2O$ (**25**)	loss: 1 H_2O	90−140		
	K−I	193	22	47
$[Tb(L^{14})(NO_3)_3]\cdot H_2O$ (**26**)	loss: 1 H_2O	90−110		
	K−I	190	30	65
$[Y(L^{14})(NO_3)_3]\cdot H_2O$ (**29**)	loss: 1 H_2O	25−80		
	K−I	189	39	84
$[Yb(L^{14})(NO_3)_3]\cdot H_2O$ (**27**)	loss: 1 H_2O	25−70		
	K−I	191	39	83
$[Lu(L^{14})(NO_3)_3]\cdot H_2O$ (**28**)	loss: 1 H_2O	25−70		
	K−I	194	17	36

[a] K = crystal, S_C = smectic C phase, S_A = smectic A phase, N = nematic phase, I = isotropic fluid. Temperatures are given as the onset of the peak (Seiko DSC 220C differential scanning calorimeter, 5 °C·min^{-1}, under N_2). The liquid-crystalline phases were identified from their optical textures: S_C = broken focal−conic fan and schlieren textures; S_A = focal−conic fan texture and homeotropic zones; N = schlieren and marbled textures. [b] Monotropic transition. [c] Second-order transition determined by polarized optical microscopy. [d] Masked by isotropization. [e] Cumulated enthalpies and entropies. [f] Approximate value: the S_C phase formed during the crystallization process. [g] Decomposition, see text.

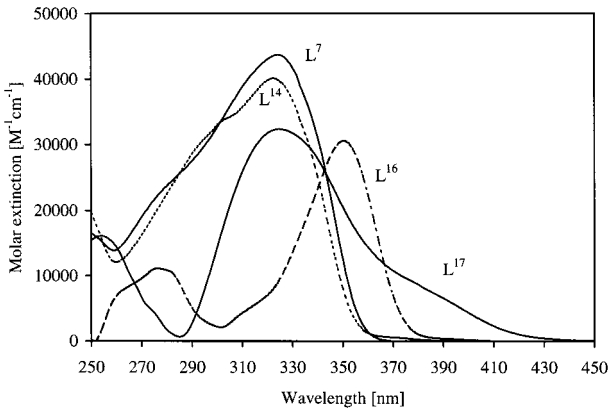

Figure 5. Absorption spectra of L^7, L^{14}, L^{16}, and L^{17} (10^{-5} M) in CH_3CN/CH_2Cl_2 (7:3) at 298 K.

substituents bound to the 5-position of the benzimidazole rings (i.e., methyl groups in L^7) destabilize the $\pi_1(A_2)$ level, leading to a shift of the $\pi\rightarrow\pi^*$ transition toward lower energy. The substitution of one hydrogen atom of these methyl groups of L^7 by a methoxy group in **8** or a 4-alkoxyphenol group in $L^{13,14}$ has only minor electronic effects, leading to very similar $\pi\rightarrow\pi^*$ transitions (Figure 5, Tables 2 and 3). However, new shoulders appear around 33 900 cm^{-1} in $L^{13,14}$ which are assigned to $\pi\rightarrow\pi^*$ transitions centered on the *p*-dihydroxyphenyl moiety by comparison with the single broad transition observed at 34 010 cm^{-1} for 1,4-dihexadecyloxybenzene.

The direct attachment of strong π-donor oxygen atoms to the 5-positions of the benzimidazole rings in L^{16} produces the expected large shift of the $\pi\rightarrow\pi^*$ transition toward lower energies (ΔE = 2480 cm^{-1} with respect to L^{14}). A weaker broad band centered at 36 230 cm^{-1} is attributed to internal transitions centered on the 4-alkoxybenzyl moiety (anisole displays a similar but structured transition at 36 900 cm^{-1}).[28] The reduced π-donor character of ester groups in L^{17} restores the usual $\pi\rightarrow\pi^*$ transition at 30 770 cm^{-1}, together with (i) a new maximum at high energy (39 370 cm^{-1}) assigned to a transition centered on the 4-alkoxybenzoic acid sidearms (*p*-anisic acid displays a broad transition at 40 160 cm^{-1})[29] and (ii) a weakly absorbing tail covering the low-energy domain (Figure 5).

The emission spectra of 10^{-5} M solutions of L^{13-17} display broad and Stokes-shifted bands originating from the $^1\pi\pi^*$ state[14,15] whose relative energies closely parallel the trends found for the absorption spectra (Table 3, Figure 6). However, **8**, L^7, and L^{16} display comparable emission intensities, while $L^{13,14,17}$ are ca. 50-fold less fluorescent. The excitation spectra recorded under analysis of the $^1\pi\pi^*$ emission closely match the absorption spectra, indicating similar UV light-harvesting properties for all studied ligands, and we conclude that nonradiative internal conversion processes are more efficient for $L^{13,14,17}$. The poor

(28) Perkampus, H. H. *UV−Vis Atlas of Organic Compounds*, 2nd ed.; VCH: Weinheim, 1992.
(29) Baker, J. W.; Barret, G. F. C.; Tweed, W. T. *J. Chem. Soc.* **1952**, 2831.

Table 2. Ligand-Centered Absorption and Emission Properties of Ligands **8**, L^7, L^{13-17}, and Complexes $[Ln(L^{14})(NO_3)_3]$ (**24**−**26**, **28**) in the Solid State[a]

compound	absorption/cm^{-1}, $\pi\rightarrow\pi^* + n\rightarrow\pi^*$	emission/cm^{-1}		lifetime/ms, τ ($^3\pi\pi^*$)
		$^1\pi\pi^*$	$^3\pi\pi^*$	
L^7	28 410	26 250	20 120	671(28)
		25 770 sh		
8	38 670	21 505 sh	20 580	572(18)
	33 820 sh	20 405	18 450 sh	
	28 170		17 270 sh	
L^{13}	38 700 sh	*b*	*b*	*b*
	28 330			
L^{14}	38 460 sh	27 320 sh	20 410	415(5)
	32 470	26 455	18 350	
	28 330	25 060 sh	17 120	
L^{16}	39 000 sh	26 180 sh	20 700	592(10)
	32 260 sh	25 380		
	26 920	24 880		
		24 100		
L^{17}	28 410 (br)	26 810 sh	19 380	614(34)
		25 970	18 450	
		24 450		
		23 200		
$[Gd(L^{14})(NO_3)_3]$ (**25**)	39 220 sh	27 760	21 800	12.0(2)
	26 670	26 315	20 120	
		25 510	18 870	
		25 000 sh	17 540 sh	
$[Lu(L^{14})(NO_3)_3]$ (**28**)	39 300 sh	24 510	20 920	76.5(6)
	26 670	23 530 sh	19 270	
			17 860	
			16 400 sh	
$[Eu(L^{14})(NO_3)_3]$ (**24**)	40 000 sh	26 385	*c*	*c*
	35 710 sh	25 000 sh		
	26 670			
$[Tb(L^{14})(NO_3)_3]$ (**26**)	39 200 sh	26 455	*c*	*c*
	33 900 sh	25 000 sh		
	26 700			

[a] Reflectance spectra recorded at 295 K, luminescence data at 77 K, and lifetime measurements at 10 K (λ_{exc} = 308 nm); sh = shoulder. [b] Too weak to be measured. [c] $^3\pi\pi^*$ luminescence quenched by transfer to Ln ion.

emissive properties of L^{14} compared to those of L^{16} strikingly demonstrate the sensitivity of electronic properties to minor structural changes, while molecular structures and thermal behavior are only marginally affected. The significantly lower oxidation potential[30] of 1,4-dialkoxybenzene (corresponding to the sidearms in L^{14}) compared to that of 4-alkoyltoluene (corresponding to the sidearms in L^{16}) might induce PET (photoinduced electron transfer) processes for $L^{13,14}$ which partially quench the luminescence.[31] Other quenching mechanisms based on some specific phonon-assisted deactivation pathways associated with the structures of L^{13}, L^{14}, and L^{17} cannot be excluded.

Emission spectra in the solid state (77 K) display structured $^1\pi\pi^*$ emission bands at energies similar to those found in solution, except for **8**, where a significant shift of the maximum toward lower energy (ΔE = 6150 cm^{-1}) is attributed to the formation of excimers in the crystal.[32] Time-resolved emission spectra (delay, 0.2−0.8 ms) exhibit faint but structured and long-lived (400−600 ms, Table 2) phosphorescence of the $^3\pi\pi^*$ states around 19 380−20 700 cm^{-1} (given for the 0−0 phonon transitions) for **8** and L^{13-17}, as previously reported for L^{3-7}.[14,15] We do not observe any significant correlation between the energy of $^3\pi\pi^*$ level and the structural variation in L^{13-17}, which indicate a common triplet state centered on the tridentate bis-(benzimidazole)pyridine units for all ligands.

Synthesis and Characterization of the Complexes $[La(L^{14})(NO_3)_3]\cdot 3H_2O$ (22) and $[Ln(L^{14})(NO_3)_3]\cdot H_2O$ (Ln = Sm, 23; Eu, 24; Gd, 25; Tb, 26; Yb, 27; Lu, 28; Y, 29). L^{14} has been selected for the investigation of 1:1 complexes with Ln(III) because of (i) its resistance toward hydrolysis, (ii) its $^1\pi\pi^*$ and $^3\pi\pi^*$ excited states located at high energy, similarly to L^7,[15] and (iii) its synthetic accessibility. The mixing of stoichiometric quantities of L^{14} and $Ln(NO_3)_3\cdot xH_2O$ (x = 2−6) in acetonitrile/dichloromethane gives the complexes $[La(L^{14})(NO_3)_3]\cdot 3H_2O$ (**22**) and $[Ln(L^{14})(NO_3)_3]\cdot H_2O$ (Ln = Sm, **23**; Eu, **24**; Gd, **25**; Tb, **26**; Yb, **27**; Lu, **28**; Y, **29**) in good yields (61−84%). The IR spectra show the characteristic ligand vibrations between 1500 and 1600 cm^{-1} (C═C, C═N stretchings) which are slightly shifted (5−10 cm^{-1}) upon complexation, together with four transitions in the range 1600−800 cm^{-1} characteristic of bidentate coordinated nitrate groups.[14] Unfortunately, we were unable to obtain X-ray quality crystals for the lipophilic complexes **22**−**29**, but yellow prisms of the model compound $[Lu(L^{13})(NO_3)_3]\cdot 2CH_3CN$ (**30**) have been grown for diffraction studies.

Crystal Structure of $[Lu(L^{13})(NO_3)_3]\cdot 3CH_3CN$ (30). The crystal structure of **30** shows it to be comprised of a neutral complex $[Lu(L^{13})(NO_3)_3]$ and three solvent molecules, of which two are slightly disordered. L^{13} adopts the expected almost planar *cis*−*cis* conformation (interplanar angles between pyridine and benzimidazole rings, 6.2° and 12.1°, Table S12) resulting from its meridional tricoordination to Lu(III) with Lu, N1, N3, and N4 distributed in a plane (maximum deviation, 0.07 Å for N4). In agreement with IR results, three bidentate nitrate groups of *pseudo*-C_{2v} symmetry occupy the vacant

(30) Effenberger, F.; Kottmann, H. *Tetrahedron* **1985**, *41*, 4171. Mattes, S. L.; Farid, S. *J. Am. Chem. Soc.* **1982**, *104*, 1454.
(31) Ghosh, P.; Bharadway, P. K.; Roy, J.; Ghosh, S. *J. Am. Chem. Soc.* **1997**, *119*, 11903 and references therein.
(32) Turro, N. J. *Modern Molecular Photochemistry*; Benjamin/Cummings Publishing Co, Inc.: Menlo Park, CA, 1978.

Table 3. Ligand-Centered Absorptions and Emission Properties of Ligands **8**, L^7, L^{13-17}, 10^{-5} M in CH_3CN/CH_2Cl_2 (7:3), and Complexes $[Ln(L^{14})(NO_3)_3]$ (**22**−**29**), 10^{-4} M in CH_3CN, at 298 K

compound	absorption/cm^{-1}, $\pi\rightarrow\pi^* + n\rightarrow\pi^*$	emission/cm^{-1}, $^1\pi\pi^*$	λ_{exc}/nm
L^7	35 715 (21 000 sh)[a]	26 315	331
	30 860 (43 700)		
8	35 700 (24 100 sh)	26 560	328
	31 250 (44 030)		
L^{13}	33 900 (29 000 sh)	26 280	328
	30 960 (38 200)		
L^{14}	33 900 (30 900 sh)	26 740	328
	31 050 (40 100)		
L^{16}	38 460 (7 230 sh)	23 980	345
	36 230 (11 470)		
	28 570 (30 830)		
L^{17}	39 370 (16 150)	23 640	334
	30 769 (32 340)		
	25 970 (7 600 sh)		
$[La(L^{14})(NO_3)_3]$ (**22**)	33 445 (25 100 sh)	*b*	
	31 450 (24 000 sh)		
	28 570 (28 500)		
$[Y(L^{14})(NO_3)_3]$ (**29**)	33 500 (25 200 sh)	*b*	
	31 450 (24 100 sh)		
	27 950 (28 400)		
$[Lu(L^{14})(NO_3)_3]$ (**28**)	33 430 (26 200)	*b*	
	31 430 (28 500 sh)		
	27 980 (28 900)		
$[Eu(L^{14})(NO_3)_3]$ (**24**)	33 300 (24 400)	*c*	
	31 420 (24 100 sh)		
	28 800 (23 200)		
$[Tb(L^{14})(NO_3)_3]$ (**25**)	33 300 (28 700)	*c*	
	31 250 (26 200 sh)		
	28 900 (25 600)		

[a] Energies are given for the maximum of the band envelope in cm^{-1}, and the molar absorption coefficient (ϵ) is given in parentheses in $M^{-1}\cdot cm^{-1}$; sh = shoulder. [b] Not measured. [c] Not detected due to $L^{14}\rightarrow$Ln(III) energy transfer.

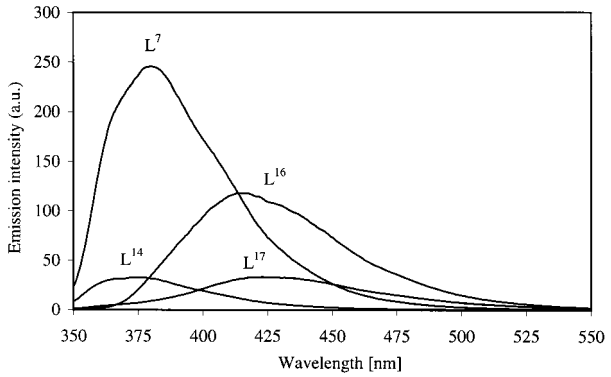

Figure 6. Emission spectra of L^7, L^{14}, L^{16}, and L^{17} (10^{-5} M) in CH_3CN/CH_2Cl_2 (7:3) at 298 K. The intensities for L^7 and L^{16} are divided by a factor of 5 (λ_{exc} are given in Table 3).

positions around the metal, leading to a low-symmetry nine-coordinate Lu atom, as similarly reported for the closely related complex $[Eu(L^5)(NO_3)_3]$.[14] Selected bond distances and bond angles are given in Table 4. Figure 7 shows the atomic numbering scheme, and Figure 8 shows an ORTEP[24] view illustrating the intermolecular stacking interactions observed in the unit cell.

The Lu−N(bzim) bond distances are ca. 0.1 Å shorter than the Lu−N(py) as a result of the larger ionic radius of Lu(III) (compared to 3d-block metal ions), as reported for the related 1:2 complex $[Lu(L^3)_2(CH_3OH)(OH_2)]^{3+}$.[15] The Lu−O distances are within standard values (2.328−2.50 Å, average 2.377 Å), except for Lu−O101, which is slightly longer. The calculated ionic radius of Lu(III) using Shannon's definition[33] and r(N) = 1.46 Å and r(O) = 1.31 Å amounts to 1.027 Å, in agreement with the expected value of 1.032 Å for nine-coordinate Lu(III).[33] The CH_2−O spacers between the benzimidazole rings and the 4-methoxyphenyl sidearms adopt a slightly staggered antiperiplanar conformation (dihedral angles C_{bzim}−C−O−C_{phenyl} = 167.8(5)° and 160.5(5)°), which results in a *quasi*-linear arrangement of the two connected aromatic moieties, as similarly found in the crystal structure of L^{13}. However, the *cis*−*cis* conformation of the coordinated bis(benzimidazole)-pyridine unit induces a U-shaped arrangement of the ligand strand associated with a reduced separation between the terminal oxygen atoms (O2···O4 = 14.90 Å) compared to that found in the free ligand L^{13} (O2···O4 = 29.07 Å). The coordinated bidentate nitrate groups fill the free space between the branches

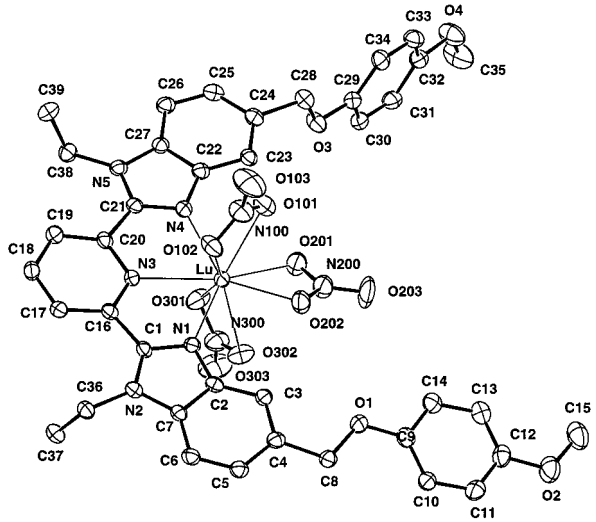

Figure 7. Atomic numbering scheme for $[Lu(L^{13})(NO_3)_3]$. Ellipsoids are represented at the 50% probability level.

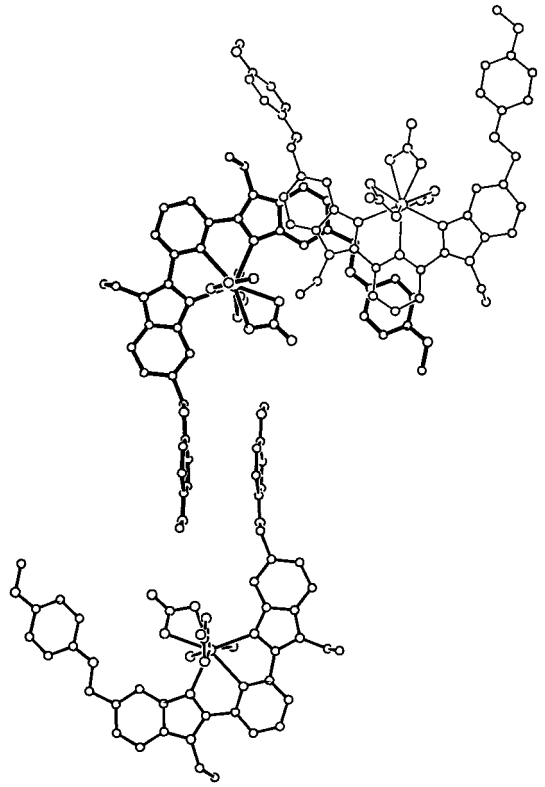

Figure 8. ORTEP[24] view of three stacked complexes in the unit cell.

(33) Shannon, R. D. *Acta Crystallogr.* **1976**, *A32*, 751.

Table 4. Selected Bond Distances (Å) and Bond Angles (Deg) for $[Lu(L^{13})(NO_3)_3]\cdot 3CH_3CN$ (**30**)

		Bond Distances			
Lu−N1	2.382(5)	Lu−O101	2.500(4)	Lu−O202	2.357(5)
Lu−N3	2.476(5)	Lu−O102	2.328(4)	Lu−O301	2.341(4)
Lu−N4	2.362(5)	Lu−O201	2.368(5)	Lu−O302	2.423(5)
C9−O1	1.372(8)	C4−C8	1.505(9)	C28−O3	1.437(7)
C8−O1	1.436(8)	C29−O3	1.373(8)	C24−C28	1.505(9)
N100−O101	1.272(9)	N200−O201	1.265(8)	N300−O301	1.253(8)
N100−O102	1.234(9)	N200−O202	1.28(1)	N300−O302	1.292(8)
N100−O103	1.216(8)	N200−O203	1.21(1)	N300−O303	1.205(9)
		Bite Angles			
N1−Lu−N3	66.2(2)	N3−Lu−N4	66.4(2)	N1−Lu−N4	132.4(2)
O101−Lu−O102	52.5(2)	O201−Lu−O202	54.2(2)	O301−Lu−O302	53.5(2)
		N−Lu−O Angles			
N1−Lu−O101	122.3(2)	N1−Lu−O201	134.1(2)	N1−Lu−O301	104.9(2)
N1−Lu−O102	74.3(2)	N1−Lu−O202	86.2(2)	N1−Lu−O302	73.8(2)
N3−Lu−O101	113.1(2)	N3−Lu−O201	155.7(2)	N3−Lu−O301	81.4(2)
N3−Lu−O102	75.7(2)	N3−Lu−O202	150.0(2)	N3−Lu−O302	106.9(2)
N4−Lu−O101	73.6(2)	N4−Lu−O201	93.0(2)	N4−Lu−O301	72.2(2)
N4−Lu−O102	89.9(2)	N4−Lu−O202	138.1(2)	N4−Lu−O302	125.4(2)
		O−Lu−O Angles			
O101−Lu−O201	70.1(2)	O101−Lu−O202	70.9(2)	O101−Lu−O301	132.7(2)
O101−Lu−O302	139.9(2)	O102−Lu−O201	118.9(2)	O102−Lu−O202	85.9(2)
O102−Lu−O301	155.3(2)	O102−Lu−O302	143.3(2)	O201−Lu−O301	80.0(2)
O201−Lu−O302	73.7(2)	O202−Lu−O302	74.3(2)	O202−Lu−O301	118.8(2)

of the U-shaped ligand strand, and two weak CH···O hydrogen bonds (C3···O202 = 3.050(8) Å, C3−H3···O202 = 139.2(3)° and C23···O201 = 3.310(8) Å, C23−H23···O201 = 134.7-(3)°) may be proposed according to recently published criteria.[34] The packing in the unit cell is controlled by two almost perpendicular π-stacking interactions. Head-to-tail dimers result from the stacking of the almost coplanar pyridine−benzimidazole-(N4,N5) unit of one complex (dihedral interplanar angle 12.1°) with the almost coplanar benzimidazole(N1,N2)−phenyl(C9−C14) unit (dihedral interplanar angle 13.3°) of the symmetry-related complex $^3/_2-x$, $^1/_2+y$, $^1/_2-z$ (average distance between stacked plane, 3.75 Å, Figure 8). Pairs of head-to-tail dimers are then formed in a perpendicular direction via a second intermolecular π-stacking interaction involving the phenyl rings (C29−C34) of two complexes related by an inversion center ($1-x$, $1-y$, $1-z$; interplane distance, 3.75 Å). This latter interaction is likely responsible for (i) the almost orthogonal arrangement (dihedral interplanar angle, 85.2°, Table S12) of the phenyl (C29−C34) and benzimidazole (N4, N5) rings within one ligand strand and (ii) the production of double layers of complexes running perpendicular to the [101] direction in the unit cell.

Photophysical Properties of Complexes $[Ln(L^{14})(NO_3)_3]\cdot H_2O$ (Ln = Eu, 24; Gd, 25; Tb, 26; Lu, 28). Upon complexation of L^{14} to Ln(III), the intense $\pi\rightarrow\pi^*$ transition centered at 31 050 cm^{-1} is split into two main components at 28 000 and 33 000 cm^{-1}, as previously reported for L^3 and L^7.[14,15] This observation reflects the electronic transformations associated with the *trans−trans* → *cis−cis* conformational change and the complexation of the lanthanide metal ions to the tridentate binding unit. Simple theoretical calculations[15] using EHMO have associated the observed variations in the electronic spectra with a reorganization of the aromatic π orbitals. The solid-state emission spectra of $[Gd(L^{14})(NO_3)_3]$ (**25**) and $[Lu(L^{14})(NO_3)_3]$ (**28**) recorded upon excitation of the ligand-centered transitions are similar to that observed for the free ligand L^{14} with $^1\pi\pi^*$ excited states located at 27 470 (Ln = Gd) and 24 510 cm^{-1} (Ln = Lu). The energy difference on going from Gd to Lu (ΔE = 2960 cm^{-1}) is reminiscent of a similar but reduced difference in the emission of the triplet states $^3\pi\pi^*$ arising at 21 800 cm^{-1} for Gd and 20 900 cm^{-1} for Lu (Table 2, values are given for the 0−0 phonon transition). These features closely match those previously discussed for $[Ln(L^3)(NO_3)_3]$ (Ln = Gd, Lu),[14] except for a blue shift of the $^1\pi\pi^*$ state in $[Ln(L^{14})(NO_3)_3]$ (ΔE = 3800 cm^{-1} for Ln = Gd and 980 cm^{-1} for Ln = Lu). In the Eu complex **24** and Tb complex **26**, the ligand-centered $^3\pi\pi^*$ phosphorescence vanishes, leading to typical metal-centered emission.[13−15] However, a residual faint emission of the $^1\pi\pi^*$ emission is observed at 77 K for both complexes (Table 2), which implies an incomplete $L^{14}\rightarrow$Ln(III) energy transfer in these complexes. Eu(III) in **24** has been used as a luminescent structural probe to investigate the nature and geometry of the coordination site.[35] Excitation via the ligand-centered $^1\pi\pi^*$ state and direct laser excitation of

Table 5. Corrected Integrated Intensities (I_{rel}) and Main Identified Eu(^7F_j) Energy Levels (cm^{-1}, j = 1−4, origin $^7F_0$) in $[Eu(L^{14})(NO_3)_3H_2O]$ (**24**) As Calculated from Luminescence Spectra in the Solid State at 10 and 295 K and in Acetonitrile Solution (295 K)

level	10 K	I_{rel}	295 K	I_{rel}	295 K[a]	I_{rel}
$^7F_0$ (λ_{exc})[b]	17 229		17 244		17 238[c]	
$^7F_1$	336	1.00	341	1.00	312	1.00
	363		366		380	
	414		418		460	
$^7F_2$	978	7.17	982	8.20	966	5.95
	1015		1032		1070	
	1032		1069		1113	
	1063				1302	
	1305					
$^7F_3$	1838	0.09	1852	0.05	1839	0.09
	1884		1890		1918	
$^7F_4$	2588	0.96	2595	1.07	2612	1.00
	2627		2681		2704	
	2668		2870		2857	
	2704		2964		2968	
	2862					
	2963					

[a] 10^{-4} M in acetonitrile. [b] Energy of the $^5D_0\leftarrow{}^7F_0$ transition (given in cm^{-1}) used as λ_{exc} for the laser-excited emission spectra. [c] Excitation via the ligand states (25 316 cm^{-1}).

(34) Steiner, T. *Chem. Commun.* **1997**, 727. Desiraju, G. R. *Acc. Chem. Res.* **1996**, *29*, 441.

Table 6. Selected Observed Lifetimes (τ, ms) of the Eu($^5D_0$) and Tb($^5D_4$) Levels in [Ln(L^{14})(NO_3)$_3$$H_2O$] (Ln = Eu, **24**; Tb, **26**) at Various Temperatures in the Solid State and in Degassed Acetonitrile Solution

compd	λ_{exc}/cm^{-1}	10 K	77 K	200 K	250 K	295 K	295 K (solution)
24	32 468	0.598(2)	0.587(2)			0.581(2)	0.728(2)
24	27 027	0.605(2)	0.610(7)			0.606(2)	
24	17 256	0.597(2)	0.585(1)			0.579(1)	
26	32 468	1.20(1)	1.19(1)	1.05(1)	0.92(1)	0.58(1)	*a*
26	27 170	1.13(1)	1.09(3)	0.77(1)	0.78(1)	0.54(1)	
26	20 492	1.16(1)	1.11(1)	0.97(1)	0.84(1)	0.55(1)	

[a] Too weak to be measured.

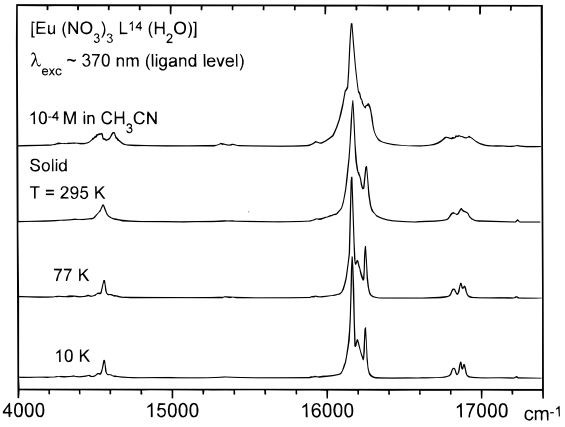

Figure 9. Emission spectra of [Eu(L^{14})(NO_3)$_3$(H_2O)] (**24**) measured under excitation through the ligand levels at various temperatures.

the $^7F_0 \rightarrow {}^5D_0$ transition between 10 and 295 K produce very similar emission spectra, except for the expected better resolution at low temperature. The maximum multiplicity ($2J + 1$) observed for the $^5D_0 \rightarrow {}^7F_j$ (j = 1, 2; Table 5) and the sizable relative intensity of the $^5D_0 \rightarrow {}^5F_2$ point to an Eu(III) ion in a low-symmetry site, which is compatible with the C_1 symmetry observed in the crystal structure of the model complex [Lu(L^{13})(NO_3)$_3$]·3CH_3CN (**30**). The lifetime of the Eu($^5D_0$) level in **24** does not display significant temperature dependence, in agreement with negligible energy back transfer to the $^3\pi\pi^*$ level located 3750 cm^{-1} above the emitting $^5D_0$ level.[36] Its short value (0.579 ms) can be compared with that found for [Eu(L^3)(NO_3)$_3$(CH_3OH)], 0.840 ms,[14] where one methanol molecule is bound to Eu(III), and points to water interaction in the first coordination sphere. The empirical equation of Horrocks and Sudnick[37] allows one to determine the number of coordinated water molecules: $q = A_{Eu}^{H_2O}(\tau_{H_2O}^{-1} - \tau_{H_2O}^{-1})$, with $A_{Eu}^{H_2O} = 1.05$. In our case, the lifetime in the absence of OH oscillators bound to Eu(III) may be estimated to lie in the range $1.11 < \tau_{D_2O} < 1.35$ ms, the lower and upper values corresponding respectively to τ measured for [Eu(L^5)(NO_3)$_3$][14] and [Eu(NO_3)$_3$(CH_3CN)$_3$][35,38] at 295 K. We find $0.87 < q < 1.04$ and conclude that [Eu(L^{14})(NO_3)$_3$]·H_2O is better formulated as [Eu(L^{14})(NO_3)$_3$(H_2O)], with one water molecule bound to Eu(III), leading to a low-symmetry 10-coordinate metal ion. Moreover, the $^5D_0 \leftarrow {}^7F_0$ excitation spectrum consists of a single band (17 244 cm^{-1}, full width at half-height (fwhh) = 7.7 cm^{-1} at 295 K), implying a unique coordination site for Eu(III). The energy of the $^5D_0 \leftarrow {}^7F_0$ transition $\tilde{\nu}$ depends on the ability of n_i coordinating atoms to produce a nephelauxetic effect δ_i:[39] $\tilde{\nu} - \tilde{\nu}_0 = C_{Cn}\sum_i n_i\delta_i$, where C_{CN} is a function of the total coordination number of the Eu(III) ion (0.95 for CN = 10) and $\tilde{\nu}_0$ = 17 374 cm^{-1} at 295 K. Taking δ_N(N-heterocyclic) = −15.3,[20,40] $\delta_O(NO_3^-)$ = −13.3,[14] and $\delta_O(H_2O)$ = −9.9,[39] we calculate $\tilde{\nu}_0$ = 17 245 cm^{-1} for 10-coordinate Eu(III) in [Eu(L^{14})(NO_3)$_3$(H_2O)] at 295 K, a value which almost exactly fits the experiment (17 244 cm^{-1}) and supports the latter formulation of the complex.

Excitation of the ligand-centered $^1\pi\pi^*$ excited state in **26** at room temperature produces only weak Tb-centered emission bands assigned to $^5D_4 \rightarrow {}^7F_j$ (j = 1−6) transitions whose intensities significantly increase upon cooling the sample (Figure F1). The lifetime of the Tb($^5D_4$) level measured under direct laser excitation of the $^5D_4 \leftarrow {}^7F_6$ transition is temperature dependent, decreasing from 1.16 ms at 10 K to 0.55 ms at 295 K (Table 6), pointing to a particular quenching process operating in this complex. Analysis of τ($^5D_4$) in the range 40−295 K according to an Arrhenius plot of the type $\ln(\tau^{-1} - \tau_0^{-1}) = A - (E_a/RT)$ (τ_0 is the lifetime in the absence of quenching process, taken here as τ at 10 K)[41] gives a straight line corresponding to an activation energy, $E_a = 200 \pm 50$ cm^{-1}, very similar to that found for Tb($^5D_4$)$\rightarrow {}^3\pi\pi^*$ energy back transfer in a Tb complex with a calixarene (E_a = 180 cm^{-1}).[41] We conclude that a related back transfer occurs in **26** as previously proposed for the analogous complex [Tb(L^3)(NO_3)$_3$(CH_3OH)].[14] Following the same reasoning as above with $A_{Tb}^{H_2O} = 4.2$,[37] τ_{H_2O} = 1.16 ms (at 10 K where no back transfer remains), and $\tau_{D_2O} \approx 1.87$ ms ([Tb(NO_3)$_3$($MeCN$)$_3$][35,38]), we find q = 1.4. As for the Eu complex, the water molecule in [Tb(L^{14})(NO_3)$_3$]·H_2O (**26**) is therefore bound in the first coordination sphere, leading to the correct formulation [Tb(L^{14})(NO_3)$_3$(H_2O)].

Thermal Behavior of Complexes [La(L^{14})(NO_3)$_3$]·3H_2O (22) and [Ln(L^{14})(NO_3)$_3$]·H_2O (Ln = Sm, 23; Eu, 24; Gd, 25; Tb, 26; Yb, 27; Lu, 28; Y, 29). According to (i) the elemental analyses of complexes **22**−**29** (Table S13), (ii) the metal-centered luminescence lifetimes for **24** and **26**, and (iii) the crystal structure of **30**, we deduce that one water molecule completes the first coordination sphere, leading to 10-coordinate metal sites for larger Ln(III) ions (Ln = La−Tb), while smaller ions (Ln = Yb, Lu, Y) are nine-coordinate, with one interstitial water molecule. The IR spectra of complexes **22**−**29** corroborate this statement and show a broad absorption in the range 3300−3500 cm^{-1} for Ln = La−Tb assigned to a coordinated water molecule, while the observation of only one narrow transition at 3640 cm^{-1} for complexes **27**−**29** is characteristic of lattice hydrogen-bonded water molecules.[42] Thermal analyses based on DSC and thermogravimetry show the latter complexes

(35) Bünzli, J.-C. G. In *Lanthanide Probes in Life, Chemical and Earth Sciences*; Bünzli, J.-C. G., Choppin, G. R., Eds.; Elsevier Publishing Co.: Amsterdam, 1989; Chapter 7.

(36) Latva, M.; Takalo, H.; Mukkala, V.-M.; Matachescu, C.; Rodriguez-Ubis, J. C.; Kankare, J. *J. Luminesc.* **1997**, *75*, 149.

(37) Horrocks, W. deW., Jr.; Sudnick, D. R. *J. Am. Chem. Soc.* **1979**, *101*, 334. Horrocks, W. deW., Jr.; Sudnick, D. R. *Science* **1979**, *206*, 1194.

(38) Bünzli, J.-C.G.; Milicic-Tang, A.; Mabillard, C. *Helv. Chim. Acta* **1993**, *76*, 1292. Bünzli, J.-C.G; Yersin, J.-R. *Inorg. Chim. Acta* **1984**, *94*, 301.

(39) Frey, S. T.; Horrocks, W. deW., Jr. *Inorg. Chim. Acta* **1995**, *229*, 383.

(40) Piguet, C.; Bünzli, J.-C. G.; Bernardinelli, G.; Hopfgartner, G.; Petoud, S.; Schaad, O. *J. Am. Chem. Soc.* **1996**, *118*, 6681.

(41) Charbonnière, L. J.; Balsiger, C.; Schenk, K. J.; Bünzli, J.-C. G. *J. Chem. Soc., Dalton Trans.* **1998**, 505.

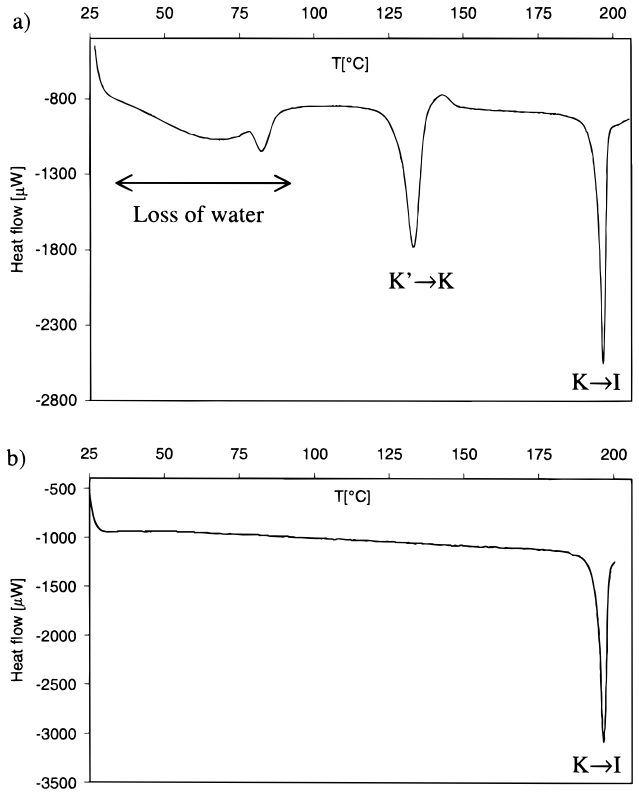

Figure 10. Differential scanning thermogramms of $[Lu(L^{14})(NO_3)_3]\cdot H_2O$ (**28**): (a) first heating process and (b) second heating process after a prior 25 °C→150 °C→25 °C cycle.

27−**29** to lose their lattice water molecule in the range 25−80 °C (Table 1). Subsequent crystal rearrangements produce complicated DSC traces during the first heating process, but meltings in the range 190−194 °C are found for the three complexes (Table 1, Figure 10a). Fast decomposition occurs in the isotropic liquid which strongly limits reversibility, but a preliminary cycle 25 °C→150 °C→25 °C leads to the exclusive observation of the endothermic isotropisation process during the second heating without complications associated with water loss and crystal rearrangements (Figure 10b). No mesophases have been detected by polarizing microscopy. For complexes **23**−**26**, the bound water molecule requires higher temperatures to be removed (90−140 °C), which supports its coordination to the metal ion, but this process is followed by a fast decomposition of the complexes on the heated plate. A related behavior is observed for $[La(L^{14})(NO_3)_3]\cdot 3H_2O$ (**22**): two interstitial water molecules are lost between 25 and 80 °C, while the coordinated water molecule is removed at 100−125 °C prior to decomposition. We conclude that no thermotropic mesophases are formed during the heating processes for **22**−**29**, but the thermal properties strongly depend on the size of Ln(III), as previously noticed in other complexes.[17] It is well established that the stability of nitrate salts varies markedly with the basicity of the metal, decomposition being significantly delayed for small cations with high positive charge.[43] This may partially explain the higher thermal stability of **27**−**29** compared to that of **22**−**26**, but we cannot exclude (i) some specific destabilization associated with the removal of the water molecule from the first coordination sphere in **22**−**26** and (ii) a partial decomplexation of the tridentate binding unit with large Ln(III) ions since weak but observable thin endotherms at 132 °C (corresponding to the melting K→S_A process of the free ligand) are systematically detected for **22**−**26** prior to decomposition.

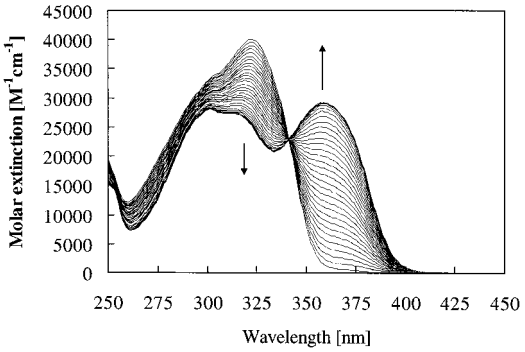

Figure 11. Spectrophotometric titration of L^{14} (10^{-4} M in CH_3CN/CH_2Cl_2 = 1:1) by $Lu(NO_3)_3\cdot 2.7H_2O$ for Lu:L^{14} ratio in the range 0.1−1.8.

Structure of Complexes $[La(L^{14})(NO_3)_3]\cdot 3H_2O$ (22) and $[Ln(L^{14})(NO_3)_3]\cdot H_2O$ (Ln = Sm, 23; Eu, 24; Gd, 25; Tb, 26; Yb, 27; Lu, 28; Y, 29) in Solution. The splitting of the ligand-centered $\pi\rightarrow\pi^*$ transition of L^{14} upon complexation to Ln(III) (Ln = La−Lu) previously discussed in the solid state can be easily monitored by spectrophotometry in solution (Figure 11). Titrations of L^{14} (10^{-4} M in 1:1 CH_3CN/CH_2Cl_2) with $Ln(NO_3)_3\cdot 3H_2O$ (Ln = La, Sm, Lu) show (i) an end point for Ln:L^{14} = 1.0 and (ii) an isobestic point at 345 nm. These observations imply the existence of only two absorbing species in solution according to equilibrium 1, and the data can be

$$Ln(NO_3)_3\cdot 3H_2O + L^{14} \rightleftharpoons [Ln(L^{14})(NO_3)_3(H_2O)_x] + (3-x)H_2O \log(\beta) \quad (1)$$

satisfactorily fitted with $\log(\beta_{La}) = 5.7(2)$, $\log(\beta_{Sm}) = 6.0(3)$, and $\log(\beta_{Lu}) = 6.5(1)$. The stability constants are comparable within experimental errors, and despite systematic better fits with Ln = Lu, no clear thermodynamic size-discriminating effect[14] is evidenced in solution (the water content of each titrated solution was similar, with H_2O:Ln ≥ 20).

^{1}H NMR titrations in $CDCl_3$ and CD_3CN confirm the formation of 1:1 complexes $[Ln(L^{14})(NO_3)_3(H_2O)_x]$ (Ln = La, Sm, Eu, Lu) in solution. However, except in one case (Ln = Lu, $CDCl_3$), two sets of signals for the same proton and corresponding to two different complexes are systematically observed. Two-dimensional {^{1}H−^{1}H}-COSY and NOEDIF spectra allow the complete attribution of the signals to two closely related C_{2v}-symmetrical complexes which do not interconvert on the NMR time scale at room temperature (seven signals observed for the aromatic protons of each complex H^{1-7}, $H^{8,9}$, and $H^{10,11}$ appear as pairs of enantiotopic protons), as mentioned previously for $[Eu(L^3)(NO_3)_3(CH_3OH)]$.[14] The complexation of the tridentate binding unit to Ln(III) is demonstrated by (i) the systematic downfield shift[14,15] of the triplet attributed of H^1 upon complexation to La, Y, and Lu and (ii) the strong NOE effects detected between $H^{8,9}$ and H^2 only compatible with a *cis*−*cis* conformation of the receptor. Table 7 reports the chemical shifts of the protons of the main complex observed in solution. The ratios of each complex within the mixture depend on the solvent used, the temperature, and the metal ion. A detailed investigation of the NMR spectra of $[Y(L^{14})(NO_3)_3]$ in CD_3CN between 253 and 323 K (Table S14) shows these ratios varying from 70:30 at 243 K to 100:0 at 323 K, pointing to complexes under thermodynamic equilibrium. Conductivity measurements for 10^{-3} M acetonitrile solution of complexes **22**−**29** at 293 K give molar conductivity Λ_M = 65(5), 77(6),

(42) Nakamoto, K. *Infrared and Raman Spectra of Inorganic and Coordination Compounds*, 3rd ed.; J. Wiley: New York, 1972; p 226.
(43) Field, B. O.; Hardy, C. J. *Q. Rev., Chem. Soc.* **1964**, *18*, 361.

Table 7. Proton NMR Shifts (with Respect to TMS) for Ligand L^{14} in $CDCl_3$ and Its Main Complexes $[Ln(L^{14})(NO_3)_3]$ (Ln = La, Sm; Y, Lu) in CD_3CN at 298 K[a]

compd	H^1	H^2	H^3	H^4	H^5	$H^{6,6'}$	$H^{7,7'}$	$H^{8,9}$	$H^{10,11}$
L^{14} [b]	8.06	8.35	7.50	7.46	7.91	6.95	6.84	4.80	5.18
$[Lu(L^{14})(NO_3)_3]$[b]	8.40	8.10	7.67	7.50	8.38	6.97	6.85	4.67	5.22
$[Lu(L^{14})(NO_3)_3]$	8.35	7.80	7.61	7.45	7.81	6.95	6.83	4.80	5.20
$[Y(L^{14})(NO_3)_3]$	8.51	8.33	7.77	7.61	8.18	6.98	6.84	4.73	5.22
$[La(L^{14})(NO_3)_3]$	8.56	8.26	7.47	7.22	7.21	6.67	6.56	4.60	4.75
$[Sm(L^{14})(NO_3)_3]$	8.73	8.39	7.06	7.89	5.08	6.42	6.66	4.63	4.44

[a] See Scheme 3 for numbering scheme. [b] In $CDCl_3$.

85(7), 70(4), 46(6), 30(6), and 28(7) Ω^{-1} mol^{-1} cm^2 for Ln = La, Sm, Eu, Gd, Y, Yb, and Lu, respectively, which are intermediate between nonelectrolyte and 1:1 electrolyte (120−160 Ω^{-1} mol^{-1} cm^2) in this solvent.[44] These results strongly suggest a partial decomplexation of the nitrate anion according to eq 2, which is corroborated by the ES-MS spectra recorded under the same conditions and showing $[Ln(L^{14})(NO_3)_2]^+$ as being the only charged complex in significant concentration.

$$[Ln(L^{14})(NO_3)_3(H_2O)_x] + nCH_3CN \rightleftharpoons [Ln(L^{14})(NO_3)_2(H_2O)_x(CH_3CN)_n]^+ + NO_3^- \quad (2)$$

We also notice that molar conductivity decreases for small Ln(III), in agreement with the expected larger electrostatic interaction. We conclude that complexes **22**−**29** exist in solution as thermodynamic mixtures of solvated and averaged C_{2v} symmetrical complexes $[Ln(L^{14})(NO_3)_3(H_2O)_x]$ and $[Ln(L^{14})(NO_3)_2(H_2O)_x(CH_3CN)_n]^+$, which do not interconvert on the NMR time scale.

Finally, emission spectra of a 10^{-4} M solution of $[Eu(L^{14})(NO_3)_3(H_2O)]$ (**24**) in acetonitrile, for which the 1:1 complex represents 91% of the ligand speciation (calculated by using $\log(\beta_{Eu}) \approx \log(\beta_{Sm}) = 6.0$), display $^5D_0 \rightarrow {}^7F_j$ transitions (j = 1−4) whose relative intensities point to low symmetry in solution compatible with C_{2v} point group.[35] Despite the lower resolution in solution, the crystal field splittings of the ^7F_j levels are different from those reported in the solid state, as revealed by the total separation of the three components of the $^7F_1$ level (148 cm^{-1} in solution compared to 77 cm^{-1} in the solid) and the variable multiplicity of $^7F_2$ and $^7F_4$ levels (Table 5, Figure 9), which are attributed to a mixture of at least two complexes with different coordination spheres around Eu(III) (eq 2). Excitation profiles of the $^7F_0 \rightarrow {}^5D_0$ transition reveal a broad band (fwhh = 28.6 cm^{-1}) centered at 17 255 cm^{-1}, compatible with a mixture of closely related complexes; for instance, we calculate[39] $\tilde{\nu}_{calc}$ = 17 245 and 17 250 cm^{-1} for $[Eu(L^{14})(NO_3)_3(H_2O)])$ and $[Eu(L^{14})(NO_3)_2(H_2O)(CH_3CN)_2]^+$, respectively. The $Eu(^5D_0)$ lifetime amounts to 0.728(2) ms, a value only somewhat longer than that measured in the solid state, indicating that the coordinated water molecule is maintained in solution and which is compatible with nitrate decomplexation.[38] The emission quantum yield relative to $[Eu(terpy)_3]^{3+}$ obtained upon irradiation of the ligand (λ_{exc} = 26 667 cm^{-1}) amounts to $\Phi_{rel} = 0.29$, an order of magnitude lower than that reported for $[Eu(L^3)(NO_3)_3(CH_3OH)]$ in the same conditions ($\Phi_{rel} = 2.74$).[14] This 10-fold decrease cannot be explained by the small difference in $Eu(^5D_0)$ lifetimes of the two complexes, but it parallels the 50-fold quenching of the fluorescence intensity ($^1\pi\pi^*$ state) observed between L^7 and L^{14}, which strongly suggests that the ligand-centered nonradiative processes associated with the elongated ligand strand L^{14} limit the uv→visible light-converting process in the Eu complex. Attempts to determine solution quantum yields for Tb in **26** failed as a result of the efficient back transfer occurring at 295 K.

Conclusions

The mesomorphism observed for L^{14-17} fully justifies our initial assumption that semilipophilic sidearms connected to the 5-position of the benzimidazole ring in L^3 may compensate the bent arrangement of the tridentate binding unit. These elongated receptors behave as rodlike molecules (I-shape) in the solid state and in the mesophase and melt at reasonable temperatures to consider them as promising receptors for metallomesogens. Two points appear to be crucial for the formation of calamitic mesophases incorporating bent tridentate bis(benzimidazole)-pyridine receptors: (i) the length and nature of the spacers between the benzimidazole rings and the phenyl sidearms, which control the degrees of freedom of the central aromatic moiety, and (ii) the conformation of the bis(benzimidazole)pyridine core, which must provide a linear arrangement of the semirigid lipophilic side chains. Our detailed photophysical investigation shows that electronic properties are also strongly affected by the choice of the spacer, which offers fascinating possibilities for the design of liquid crystals with predetermined photophysical properties. The drastic structural changes associated with the *trans*−*trans* → *cis*−*cis* conformational interconversion occurring upon complexation of the tridentate binding unit produces a U-shaped organization of the ligand strand in $[LnL^{14}(NO_3)_3(H_2O)_x]$ (Ln = La−Tb, x = 1; Ln = Yb, Lu, Y, x = 0), being located in the resulting internal cavity. For larger Ln(III) ions (La−Tb), decomposition of the complexes occurs at rather low temperature (∼120−130 °C), thus preventing a detailed investigation of the thermal behavior. For smaller ions (Ln = Gd−Lu, Y), the increased stability resulting from a combination of improved electrostatic effects with a reduced coordination number (no water molecule bound to Ln(III)) delays the decomposition processes and allows the observation of a simple isotropization processes around 190 °C. No mesogenic behavior is observed for the complexes, and we tentatively assign this failure essentially to the reduced length/width ratio associated with the U-shaped arrangement of the ligand strand in the complex. These results refute the simplistic idea that mesogenic ligands lead to metallomesogens upon complexation,[1−3] although this approach remains justified when no major geometrical or structural changes occur upon complexation, as found for *pseudo*-linear binding units.[8,9]

Experimental Section

Solvents and starting materials were purchased from Fluka AG (Buchs, Switzerland) and used without further purification, unless otherwise stated. Acetonitrile, dichloromethane, *N*,*N*-dimethylformamide (DMF), dimethyl sulfoxide (DMSO), and triethylamine were distilled from CaH_2, thionyl chloride from elemental sulfur. The nitrate salts $Ln(NO_3)_3 \cdot nH_2O$ (Ln = La to Lu) were prepared from the corresponding oxides (Glucydur, 99.99%) according to literature

(44) Geary, W. J. *Coord. Chem. Rev.* **1971**, *7*, 81.

procedures.[14] Silica gel (Merck 60, 0.040−0.060 mm) was used for preparative column chromatography.

Preparation of 1-Chloro-4-methoxymethyl-2-nitrobenzene (2). KOH (85%, 7.0 g, 107 mmol) was dissolved in freshly distilled DMSO, and **1** (5.0 g, 27 mmol) and methyl iodide (9.12 g, 64.2 mmol) were added in this order. After 1 h of stirring at room temperature, water (60 mL) was added, and the resulting mixture was extracted with dichloromethane (3 × 40 mL). The combined organic fractions were washed with water (5 × 30 mL), dried (Na_2SO_4), and evaporated, and the residual oil was distilled (90 °C, 10^{-2} Torr) to give 4.48 g (22.2 mmol, yield 83%) of **2** as a colorless liquid. ^{1}H NMR in $CDCl_3$: δ 3.44 (3H, s), 4.49 (2H, s), 7.48 (1H, dd, $J^3 = 8$ Hz, $J^4 = 2$ Hz), 7.53 (1H, d, $J^3 = 8$ Hz), 7.85 (1H, d, $J^4 = 2$ Hz). EI-MS: *m*/*z* 201/203 (M^+).

Preparation of *N*-Ethyl-(4-methoxymethyl-2-nitrophenyl)amine (3). 1-Chloro-4-methoxymethyl-2-nitrobenzene (**2**, 4.48 g, 22.2 mmol) and ethylamine (70% in water, 50 mL) were heated in an autoclave at 100 °C for 12 h. The dark mixture was evaporated to dryness, extracted with dichloromethane (100 mL), filtered over Celite, and washed with half-saturated aqueous NH_4Cl solution (30 mL). The organic phase was dried (Na_2SO_4), the solvent evaporated, and the resulting oil distilled (140 °C, 10^{-2} Torr) to give 3.9 g (18.6 mmol, yield 84%) of **3** as a red oil. ^{1}H NMR in $CDCl_3$: δ 1.37 (3H, t, $J^3 = 7$ Hz), 3.36 (3H, s), 3.37 (2H, q, $J^3 = 7$ Hz), 4.34 (2H, s), 6.85 (1H, d, $J^3 = 8$ Hz), 7.45 (1H, dd, $J^3 = 8$ Hz, $J^4 = 2$ Hz), 8.01 (1H, s br), 8.14 (1H, d, $J^4 = 2$ Hz). EI-MS: *m*/*z* 210 (M^+). The same procedure was used for the preparation of *N*-ethyl-(4-methoxy-2-nitrophenyl)amine (**5**) from 4-chloro-3-nitroanisole (**4**) yielding red microcrystals (from CH_2Cl_2/hexane, yield 90%). ^{1}H NMR in $CDCl_3$: δ 1.36 (3H, t, $J^3 = 7$ Hz), 3.35 (2H, q, $J^3 = 7$ Hz), 3.80 (3H, s), 6.83 (1H, d, $J^3 = 9$ Hz), 7.16 (1H, dd, $J^3 = 9$ Hz, $J^4 = 3$ Hz), 7.62 (1H, d, $J^4 = 3$ Hz), 7.94 (1H, s br). EI-MS: *m*/*z* 196.2 (M^+).

Preparation of Bis[*N*-ethyl-*N*-(4-methoxymethyl-2-nitrophenyl)]-pyridine-2,6-dicarboxamide (6). Pyridine-2,6-dicarboxylic acid (4.38 g, 26 mmol) and DMF (50 μL) were refluxed in freshly distilled thionyl chloride (35 mL) for 45 min. Excess thionyl chloride was distilled from the reaction mixture, which was then coevaporated with dry dichloromethane (2 × 20 mL) and dried under vacuum. *N*-Ethyl-(4-methoxymethyl-2-nitrophenyl)amine (**3**) (5.51 g, 26.2 mmol) and triethylamine (39.4 mL, 0.26 mol) were refluxed in dry dichloromethane (15 mL), and the solid 2,6-dichlorocarboxypyridine previously prepared was added. The resulting mixture was refluxed for 8 h, evaporated to dryness, and partitioned between dichloromethane (3 × 30 mL) and half-saturated aqueous NH_4Cl (30 mL). The combined organic fractions were evaporated to dryness, and the crude product was purified by column chromatography (silica gel; CH_2Cl_2/MeOH 100:0→99.5:0.5) to give 4.53 g (8.2 mmol, yield 62%) of **6** as a pale yellow powder. ^{1}H NMR in $CDCl_3$: δ 1.00−1.28 (6H, m), 3.32−3.45 (6H, m), 3.48−4.26 (4H, m), 4.40−4.56 (4H, m), 7.09 (2H, m), 7.40 (2H, m), 7.38 (2H, m), 7.53 (1H, m), 7.88 (2H, m). ES-MS (CH_2Cl_2): *m*/*z* 552.3 ($[M + H]^+$). The same procedure was used for the preparation of bis-[*N*-ethyl-*N*-(4-methoxy-2-nitrophenyl)]pyridine-2,6-dicarboxamide (**7**) as a pale yellow powder from **5** (CC, silica gel; CH_2Cl_2/MeOH 99.8:0.2→99:1, yield 75%). ^{1}H NMR in $CDCl_3$: δ 1.01−1.24 (6H, m), 3.46−4.27 (4H, m), 3.75−3.91 (6H, m), 6.95 (2H, m), 7.04 (2H, m), 7.39 (2H, m), 7.52 (1H, m), 7.82 (2H, m). ES-MS (CH_2Cl_2): *m*/*z* 524.2 ($[M + H]^+$).

Preparation of 2,6-Bis-(1-ethyl-5-methoxymethyl-benzimidazol-2-yl)pyridine (8). Bis[*N*-ethyl-*N*-(4-methoxymethyl-2-nitrophenyl)]-pyridine-2,6-dicarboxamide (**6**, 3.09 g, 5.6 mmol) was dissolved in ethanol/water (480 mL:120 mL). Activated iron powder (6.26 g, 0.11 mol) and concentrated hydrochloric acid (37%, 15 mL, 0.18 mol) were added, and the mixture was refluxed for 12 h. The excess of iron was filtered and ethanol distilled under vacuum. The resulting mixture was poured into CH_2Cl_2 (200 mL), $Na_2H_2EDTA{\cdot}2H_2O$ (30 g) dissolved in water (150 mL) was added, and the resulting stirred mixture was neutralized (pH = 8.5) with 24% aqueous NH_4OH. Concentrated hydrogen peroxide (30%, 5 mL) was added under vigorous stirring. After 15 min, the organic layer was separated and the aqueous phase extracted with CH_2Cl_2 (3 × 40 mL). The combined organic phases were dried (Na_2SO_4) and evaporated to dryness, and the crude residue was purified by column chromatography (silica gel; CH_2Cl_2/MeOH 99:1→97:3) and crystallized from CH_2Cl_2/hexane to give 2.05 g (4.5 mmol, yield 80%) of **8** as white microcrystals. ^{1}H NMR in $CDCl_3$: δ 1.37 (6H, t, $J^3 = 7$ Hz), 3.42 (6H, s), 4.63 (4H, s), 4.80 (4H, q, $J^3 = 7$ Hz), 7.39 (2H, dd, $J^3 = 8$ Hz, $J^4 = 1$ Hz), 7.47 (2H, d, $J^3 = 8$ Hz), 7.82 (2H, d, $J^4 = 1$ Hz), 8.06 (1H, t, $J^3 = 8$ Hz), 8.35 (2H, d, $J^3 = 8$ Hz). ES-MS (CH_2Cl_2): *m*/*z* 478.3 ($[M + Na]^+$). The same procedure was used for the preparation of 2,6-bis(1-ethyl-5-methoxybenzimidazol-2-yl)pyridine (**9**) as white microcrystals from **7** (CC, silica gel; CH_2Cl_2/MeOH 98:2, yield 60%). ^{1}H NMR in $CDCl_3$: δ 1.36 (6H, t, $J^3 = 7$ Hz), 3.91 (6H, s), 4.79 (4H, q, $J^3 = 7$ Hz), 7.03 (2H, dd, $J^3 = 9$ Hz, $J^4 = 2$ Hz), 7.34 (2H, d, $J^4 = 2$ Hz), 7.36 (2H, d, $J^3 = 9$ Hz), 8.03 (1H, t, $J^3 = 8$ Hz), 8.32 (2H, d, $J^3 = 8$ Hz). ES-MS (CH_2Cl_2): *m*/*z* 428.3 ($[M + H]^+$).

Preparation of 2,6-Bis(1-ethyl-5-bromomethylbenzimidazol-2-yl)-pyridine (10). 2,6-Bis(1-ethyl-5-methoxymethylbenzimidazol-2-yl)-pyridine (**8**, 200 mg, 0.439 mmol) was dissolved in dichloromethane (25 mL), and boron tribromide (1 M in CH_2Cl_2, 8.78 mL, 0.878 mmol) was added via a syringe under an inert atmosphere. After 3 h of stirring at room temperature, water (30 mL) was added, and the aqueous phase was neutralized until pH = 7−8 with saturated aqueous $NaHCO_3$. The organic layer was separated and the aqueous phase extracted with CH_2Cl_2 (3 × 30 mL). The combined organic phases were dried (Na_2SO_4), concentrated to 5 mL, filtered on silica gel (CH_2Cl_2/MeOH 97:3), and evaporated to dryness. The crude residue was crystallized from CH_2Cl_2/hexane (1:1) to give 223 mg (0.404 mmol, yield 92%) of **10** as white microcrystals. ^{1}H NMR in $CDCl_3$: δ 1.37 (6H, t, $J^3 = 7$ Hz), 4.74 (4H, s), 4.77 (4H, q, $J^3 = 7$ Hz), 7.43 (2H, dd, $J^3 = 8$ Hz, $J^4 = 1$ Hz), 7.47 (2H, d, $J^3 = 8$ Hz), 7.88 (2H, s br), 8.07 (1H, t, $J^3 = 8$ Hz), 8.34 (2H, d, $J^3 = 8$ Hz). ES-MS (CH_2Cl_2): *m*/*z* 552/554 ($[M + H]^+$). The same procedure was used for the preparation of 2,6-bis(1-ethyl-5-hydroxybenzimidazol-2-yl)pyridine (**11**) from **9**, except for the workup procedure. After neutralization with saturated aqueous $NaHCO_3$, the crude solution was evaporated to dryness. The solid residue was dissolved in a minimum of CH_2Cl_2/CH_3OH (1:1), silica gel (10 g) was added, and the solvent was evaporated. The resulting powder was deposited on top of the column and chromatographed (silica gel; CH_2Cl_2/MeOH 99:1→95:5) and then crystallized from CH_2Cl_2/CH_3OH (1:1) to give **8** as a pale yellow powder (yield 70%). Mp > 250 °C. ^{1}H NMR in DMSO-d_6: δ 1.27 (6H, t, $J^3 = 7$ Hz), 4.79 (4H, q, $J^3 = 7$ Hz), 6.85 (2H, dd, $J^3 = 9$ Hz, $J^4 = 2$ Hz), 7.00 (2H, d, $J^4 = 2$ Hz), 7.50 (2H, d, $J^3 = 9$ Hz), 8.16 (1H, t, $J^3 = 8$ Hz), 8.29 (2H, d, $J^3 = 8$ Hz), 9.20 (2H, s). ES-MS (CH_2Cl_2): *m*/*z* 400.2 ($[M + H]^+$).

Preparation of 3,4-Bis(dodecyloxy)benzoic Acid Dodecyl Ester (13). 3,4-Dihydroxybenzoic acid (**12**, 1.0 g, 6.48 mmol) and 1-bromododecane (5.16 g, 20.7 mmol) were dissolved in DMSO (15 mL), and powdered potassium hydroxide (85%, 1.28 g, 19.4 mmol) was added in one portion. After 12 h of stirring at 80 °C under an inert atmosphere, half-saturated aqueous NH_4Cl (30 mL) was added, and the resulting mixture was extracted with dichloromethane (3 × 30 mL). The combined organic layer was washed with water (5 × 30 mL), dried (Na_2SO_4), and evaporated. The crude residue was purified by column chromatography (silica gel; hexane/CH_2Cl_2 90:10) to give 3.43 g (5.2 mmol, yield 80%) of **13** as a white powder. Mp 64−65 °C. ^{1}H NMR in $CDCl_3$: δ 0.90 (9H, t, $J^3 = 7$ Hz), 1.2−2.0 (60H, m), 4.04 (2H, t, $J^3 = 7$ Hz), 4.05 (2H, t, $J^3 = 7$ Hz), 4.28 (2H, t, $J^3 = 7$ Hz), 6.86 (1H, d, $J^3 = 8$ Hz), 7.54 (1H, d, $J^4 = 2$ Hz), 7.64 (1H, dd, $J^3 = 8$ Hz, $J^4 = 2$ Hz). EI-MS: *m*/*z* 658.7 (M^+).

Preparation of 3,4-Bis(dodecyloxy)benzoic Acid (14). 3,4-bis-(dodecyloxy)benzoic acid dodecyl ester (**13**, 3.43 g, 5.21 mmol) and powdered potassium hydroxide (85%, 7.92 g, 0.2 mol) were refluxed in ethanol/water (1:1, 60 mL) for 12 h. Ethanol was distilled and the pH adjusted to 3.0 with concentrated hydrochloric acid (37%). The resulting aqueous phase was extracted with dichloromethane (3 × 30 mL), and the combined organic phases were dried (Na_2SO_4) and evaporated to dryness. The crude product was crystallized from hot ethanol to give 2.02 g (4.11 mmol, yield 79%) of **14** as a white powder. Mp 58−59 °C. ^{1}H NMR in $CDCl_3$: δ 0.88 (6H, t, $J^3 = 7$ Hz), 1.2−1.9 (40H, m), 4.05 (2H, t, $J^3 = 7$ Hz), 4.07 (2H, t, $J^3 = 7$ Hz), 6.89 (1H, d, $J^3 = 8$ Hz), 7.58 (1H, d, $J^4 = 2$ Hz), 7.72 (1H, dd, $J^3 = 8$ Hz, $J^4 = 2$ Hz). EI-MS: *m*/*z* 490.4 (M^+).

Preparation of 4-Dodecyloxyphenol (17). *p*-Hydroquinone (5.5 g, 50 mmol), 1-bromododecane (12.46 g, 50 mmol), and potassium hydrogen carbonate (5.0 g, 50 mmol) were refluxed in dioxane/water (1:1, 200 mL) for 12 h. Dioxane was distilled and the pH adjusted to 3.0 with concentrated hydrochloric acid (37%). The resulting aqueous phase was extracted with dichloromethane (3 × 30 mL), and the combined organic phases were dried (Na_2SO_4) and evaporated to dryness. The crude product was purified by column chromatography (silica gel; CH_2Cl_2) to give 4.2 g (14.6 mmol, yield 29%) of **13** as a white powder. Mp 74−75 °C. ^{1}H NMR in $CDCl_3$: δ 0.88 (3H, t, J^3 = 7 Hz), 1.25−1.75 (20H, m), 3.89 (2H, t, J^3 = 7 Hz), 4.42 (1H, s), 6.75 (2H, dd, J^3 = 9 Hz, J^4 = 2 Hz), 6.78 (2H, dd, J^3 = 9 Hz, J^4 = 2 Hz). EI-MS: *m*/*z* 278.3 (M^+). The same procedure was used to prepare **18** from *p*-hydroquinone and 1-bromohexadecane (yield = 20%). Mp 85 °C. ^{1}H NMR in $CDCl_3$: δ 0.88 (3H, t, J^3 = 7 Hz), 1.25−1.75 (29H, m), 3.89 (2H, t, J^3 = 7 Hz), 6.75 (2H, dd, J^3 = 9 Hz, J^4 = 2 Hz), 6.78 (2H, dd, J^3 = 9 Hz, J^4 = 2 Hz). EI-MS: *m*/*z* 334 (M^+).

Preparation of 4-Dodecyloxybenzyl Alcohol (20). $LiAlH_4$ (247 mg, 6.53 mmol) was dissolved in dry tetrahydrofuran (90 mL), and 4-dodecyloxybenzoic acid (**19**, 2.0 g, 6.53 mmol) dissolved in tetrahydrofuran (10 mL) was slowly added under an inert atmosphere. The resulting mixture was refluxed for 10 h. The remaining $LiAlH_4$ was destroyed with an excess of water, and the resulting heterogeneous mixture was evaporated to dryness and partitioned between CH_2Cl_2 and water. The organic phase was carefully separated and the aqueous phase extracted with dichloromethane (3 × 30 mL), and the combined organic phases were filtered, dried (Na_2SO_4), and evaporated to dryness. The crude product was crystallized from CH_2Cl_2/hexane to give 1.6 g (5.48 mmol, yield 84%) of **20** as a white powder. Mp 67 °C. ^{1}H NMR in $CDCl_3$: δ 0.88 (3H, t, J^3 = 7 Hz), 1.3−1.8 (20H, m), 3.95 (2H, t, J^3 = 7 Hz), 4.62 (2H, s), 6.88 (2H, d, J^3 = 9 Hz), 7.28 (2H, dd, J^3 = 9 Hz). EI-MS: *m*/*z* 292 (M^+).

Preparation of 4-Dodecyloxybenzyl Bromide (21). 4-Dodecyloxybenzyl alcohol **(20**, 1.2 g, 4.2 mmol) and phosphorus tribromide (550 mg, 2.04 mmol) were refluxed for 15 h in dichloromethane (75 mL). Excess PBr_3 was hydrolyzed with water (20 mL) and brine (80 mL). The organic phase was separated and the aqueous phase extracted with dichloromethane (3 × 30 mL), and the combined organic phases were dried (Na_2SO_4) and evaporated to dryness. The crude product was crystallized from CH_2Cl_2 to give 1.46 g (4.10 mmol, yield 99%) of **21** as white microcrystals. Mp 42−43 °C. ^{1}H NMR in $CDCl_3$: δ 0.88 (3H, t, J^3 = 7 Hz), 1.3−1.8 (20H, m), 3.95 (2H, t, J^3 = 7 Hz), 4.51 (2H, s), 6.85 (2H, d, J^3 = 9 Hz), 7.30 (2H, dd, J^3 = 9 Hz). EI-MS: *m*/*z* 354/356 (M^+).

Preparation of 2,6-Bis[1-ethyl-5-(4-dodecyloxybenzoic acid) methyl ester benzimidazol-2-yl]pyridine (L^{11}). 4-Dodecyloxybenzoic acid (**19**, 336 mg, 1.09 mmol) and tetra-*n*-butylammonium hydroxide (0.1 M in 2-propanol/methanol, 10.9 mL, 1.09 mmol) were dissolved in dichloromethane (10 mL). The solvent was evaporated to dryness and the resulting salt dried under vacuum. 2,6-Bis(1-ethyl-5-bromomethylbenzimidazol-2-yl)pyridine (**10**, 200 mg, 0.361 mmol) in dry dichloromethane (20 mL) was poured onto the salt under an inert atmosphere and stirred for 48 h. Half-saturated aqueous NH_4Cl (50 mL) was added, the organic layer separated, and the aqueous phase extracted with CH_2Cl_2 (3 × 30 mL). The combined organic phases were dried (Na_2SO_4) and evaporated to dryness, and the crude residue was purified by column chromatography (silica gel; CH_2Cl_2/MeOH 100:0→99:1) to give 370 mg (0.369 mmol, yield 84%) of L^{11} as a white precipitate. Mp 103−104 °C. ^{1}H NMR in $CDCl_3$: δ 0.88 (6H, t, J^3 = 7 Hz), 1.37 (6H, t, J^3 = 7 Hz), 1.1−1.8 (40H, m), 4.00 (4H, t, J^3 = 7 Hz), 4.80 (4H, q, J^3 = 7 Hz), 5.50 (4H, s), 6.90 (4H, d, J^3 = 9 Hz), 7.46 (2H, d, J^3 = 8 Hz), 7.50 (2H, d, J^3 = 8 Hz), 7.97 (2H, s), 8.02 (4H, d, J^3 = 9 Hz), 8.07 (1H, t, J^3 = 8 Hz), 8.36 (2H, d, J^3 = 8 Hz). ^{13}C NMR in $CDCl_3$: δ 14.18, 15.51 (primary C); 22.74, 26.03, 29.16, 29.41, 29.63, 29.69, 31.96, 39.99, 66.87, 68.26 (secondary C); 110.37, 114.09, 120.25, 122.38, 124.15, 125.82, 131.77, 138.00 (tertiary C); 131.21, 143.01, 145.69, 149.92, 150.48, 163.07, 166.40, 180.97 (quaternary C). ES-MS (CH_2Cl_2): *m*/*z* 1004.6 ($[M + H]^+$).

Preparation of Ligands L^{12}−L^{15}. The same procedure as above was used for the syntheses of 2,6-bis{1-ethyl-5-[3,4-bis(dodecyloxy)-benzoic acid] methyl ester benzimidazol-2-yl}pyridine (L^{12}, yield 80%) and 2,6-bis{1-ethyl-5-[4-(*R*-oxy)phenoxymethyl]benzimidazol-2-yl}-pyridine (R = methyl, L^{13}, yield 84%; R = dodecyl, L^{14}, yield 82%; and R = hexadecyl, L^{15}, yield 79%) with respectively **14**, **16**−**18** as sidearms.

L^{12}. Mp 89 °C. ^{1}H NMR in $CDCl_3$: δ 0.87 (12H, t, J^3 = 7 Hz), 1.42 (6H, t, J^3 = 7 Hz), 1.2−1.8 (80H, m), 4.03 (4H, t, J^3 = 7 Hz), 4.04 (4H, t, J^3 = 7 Hz), 4.80 (4H, q, J^3 = 7 Hz), 5.51 (4H, s), 6.85 (2H, d, J^3 = 9 Hz), 7.49 (4H, m), 7.58 (2H, d, J^4 = 2 Hz), 7.70 (2H, dd, J^3 = 9 Hz, J^4 = 2 Hz), 8.00 (2H, s), 8.10 (1H, t, J^3 = 8 Hz), 8.35 (2H, d, J^3 = 8 Hz). ^{13}C NMR in $CDCl_3$: δ 14.15, 15.47 (primary C); 22.73, 26.01, 29.10, 29.24, 29.41, 29.43, 29.66, 29.80, 31.96, 40.07, 66.86, 69.05, 69.38 (secondary C); 110.45, 111.93, 114.48, 120.12, 122.43, 123.78, 124.48, 126.18, 138.42 (tertiary C); 131.62, 135.65, 148.58, 149.59, 150.12, 153.37, 166.46, 180.97 (quaternary C). ES-MS (CH_2Cl_2): *m*/*z* 1372.9 ($[M + H]^+$).

L^{13}. Mp 195 °C. ^{1}H NMR in $CDCl_3$: δ 1.37 (6H, t, J^3 = 7 Hz), 3.77 (6H, s), 4.80 (4H, q, J^3 = 7 Hz), 5.19 (4H, s), 6.84 (4H, d, J^3 = 9 Hz), 6.96 (4H, d, J^3 = 8 Hz), 7.46 (2H, d, J^3 = 8 Hz), 7.50 (2H, d, J^3 = 8 Hz), 7.92 (2H, s), 8.06 (1H, t, J^3 = 8 Hz), 8.35 (2H, d, J^3 = 8 Hz). ^{13}C NMR in $CDCl_3$: δ 15.49, 55.77 (primary C); 22.75, 39.97, 71.15 (secondary C); 110.46, 114.69, 115.99, 119.69, 123.58, 125.79, 135.77 (tertiary C); 132.13, 138.18, 142.90, 149.90, 150.37, 153.00, 153.90 (quaternary C). ES-MS (CH_2Cl_2): *m*/*z* 640.1 ($[M + H]^+$).

L^{14}. Mp 188 °C. ^{1}H NMR in $CDCl_3$: δ 0.88 (6H, t, J^3 = 7 Hz), 1.42 (6H, t, J^3 = 7 Hz), 1.2−1.8 (40H, m), 3.90 (4H, t, J^3 = 7 Hz), 4.80 (4H, q, J^3 = 7 Hz), 5.18 (4H, s), 6.84 (4H, d, J^3 = 9 Hz), 6.95 (4H, d, J^3 = 8 Hz), 7.46 (2H, d, J^3 = 8 Hz), 7.50 (2H, d, J^3 = 8 Hz), 7.97 (2H, s), 8.06 (1H, t, J^3 = 8 Hz), 8.35 (2H, d, J^3 = 8 Hz). ^{13}C NMR in $CDCl_3$: δ 14.17, 15.49 (primary C); 22.73, 26.10, 29.45, 29.65, 31.96, 39.97, 66.68, 71.13 (secondary C); 110.44, 115.44,115.94, 119.68, 123.60, 125.80, 138.18 (tertiary C); 132.20, 135.75, 142.05, 149.93, 150.33, 152.88, 153.53 (quaternary C). ES-MS (CH_2Cl_2): *m*/*z* 948.5 ($[M + H]^+$).

L^{15}. Mp 184 °C. ^{1}H NMR in $CDCl_3$: δ 0.88 (6H, t, J^3 = 7 Hz), 1.42 (6H, t, J^3 = 7 Hz), 1.2−1.8 (56H, m), 3.90 (4H, t, J^3 = 7 Hz), 4.80 (4H, q, J^3 = 7 Hz), 5.18 (4H, s), 6.84 (4H, d, J^3 = 9 Hz), 6.95 (4H, d, J^3 = 8 Hz), 7.46 (2H, d, J^3 = 8 Hz), 7.50 (2H, d, J^3 = 8 Hz), 7.97 (2H, s), 8.06 (1H, t, J^3 = 8 Hz), 8.35 (2H, d, J^3 = 8 Hz). ^{13}C NMR in $CDCl_3$: δ 14.17, 15.49 (primary C); 22.73, 26.10, 29.45, 29.65, 31.96, 39.97, 66.68, 71.13 (secondary C); 110.44, 115.44, 115.94, 199.68, 123.60, 125.80, 138.18 (tertiary C); 132.20, 135.75, 142.95, 149.93, 150.33, 152.88, 153.53 (quaternary C). ES-MS (CH_2Cl_2): *m*/*z* 1060.5 ($[M + H]^+$).

Preparation of 2,6-Bis[1-ethyl-5-(4-dodecyloxy)benzyloxybenzimidazol-2-yl]pyridine (L^{16}). A suspension of 2,6-bis(1-ethyl-5-hydroxy-benzimidazol-2-yl)pyridine (**11**, 300 mg, 0.751 mmol) in dichloromethane (10 mL) was reacted with tetra-*n*-butylammonium hydroxide (0.38 M in methanol, 4.34 mL, 1.65 mmol). After complete solubilization, the solvent was evaporated and the resulting salt dried under vacuum and redissolved in dry dichloromethane (20 mL). 4-Dodecyloxybenzyl bromide (**21**, 586 mg, 1.65 mmol) in dry dichloromethane (10 mL) was added and the solution refluxed for 10 h under an inert atmosphere. The standard workup described for L^{11} gave 410 mg (0.43 mmol, yield 57%) of L^{16}, which was crystallized from CH_2Cl_2/hexane. Mp 193 °C. ^{1}H NMR in $CDCl_3$: δ 0.88 (6H, t, J^3 = 7 Hz), 1.40 (6H, t, J^3 = 7 Hz), 1.3−1.8 (40H, m), 3.96 (4H, t, J^3 = 7 Hz), 4.77 (4H, q, J^3 = 7 Hz), 5.08 (4H, s), 6.91 (4H, d, J^3 = 9 Hz), 7.10 (2H, dd, J^3 = 8 Hz, J^4 = 2 Hz), 7.36 (2H, d, J^3 = 8 Hz), 7.40 (4H, d, J^3 = 8 Hz), 7.42 (2H, s), 8.04 (1H, t, J^3 = 8 Hz), 8.32 (2H, d, J^3 = 8 Hz). ^{13}C NMR in $CDCl_3$: δ 14.17, 15.56 (primary C); 22.74, 26.00, 29.41, 31.96, 39.92, 68.10, 70.59 (secondary C); 103.61, 110.72, 114.63, 114.95, 125.47, 129.34, 138.00 (tertiary C); 128.90, 155.81, 159.07 (quaternary C). ES-MS (CH_2Cl_2): *m*/*z* 948.3 ($[M + H]^+$). The same procedure was used for the syntheses of 2,6-bis[1-ethyl-5-(4-dodecyloxybenzoic ester) benzimidazol-2-yl]pyridine (L^{17}) from the acyl chloride of **19** (yield 60%).

L^{17}. Mp 226 °C. ^{1}H NMR in $CDCl_3$: δ 0.88 (6H, t, J^3 = 7 Hz), 1.40 (6H, t, J^3 = 7 Hz), 1.3−1.8 (40H, m), 4.60 (4H, t, J^3 = 7 Hz), 4.81 (4H, q, J^3 = 7 Hz), 7.00 (4H, d, J^3 = 9 Hz), 7.23 (2H, dd, J^3 = 8 Hz, J^4 = 2 Hz), 7.51 (2H, d, J^3 = 8 Hz), 7.68 (4H, d, J^4 = 2 Hz), 8.08 (1H, t, J^3 = 8 Hz), 8.10 (4H, d, J^3 = 9 Hz), 8.36 (2H, d, J^3 = 8

Table 8. Summary of Crystal Data, Intensity Measurements, and Structure Refinement for L,[13] L[16], and $[Lu(L^{13})(NO_3)_3]\cdot 3CH_3CN$ (**30**)

	L^{13}	L^{16}	$[Lu(L^{13})(NO_3)_3]$
formula	$C_{39}H_{37}N_5O_4$	$C_{61}H_{81}N_5O_4$	$LuC_{45}H_{46}N_{11}O_{13}$
mol wt	639.8	948.3	1123.9
cryst syst	triclinic	triclinic	monoclinic
space group	$P\bar{1}$	$P\bar{1}$	$C2/c$
a, Å	10.315(1)	8.7732(8)	21.273(1)
b, Å	11.8767(7)	10.686(1)	19.9614(6)
c, Å	14.170(2)	29.997(5)	23.0538(7)
α, deg	105.076(5)	90.134(8)	90
β, deg	108.972(6)	94.383(8)	102.322(3)
γ, deg	95.109(5)	108.593(8)	90
V, Å^3	1556.2(2)	2656.6(6)	9564.0(6)
Z	2	2	8
D_{calc}, g·cm^{-3}	1.37	1.19	1.56
$F(000)$	676	1028	4544
$\mu_{Cu\ K\alpha}$, mm^{-1}	0.721	0.574	4.595
abs, A^*_{min}/A^*_{max}	1.102/1.186	1.042/1.209	2.698/3.976
cryst size, mm	0.15 × 0.20 × 0.37	0.076 × 0.22 × 0.60	0.15 × 0.17 × 0.17
temp, K	200	170	200
reflns measured	3741	6658	5622
θ range	$3° < 2\theta < 105°$	$3° < 2\theta < 110°$	$3° < 2\theta < 105°$
h,k,l range	$-10 < h < 10$	$-9 < h < 9$	$-21 < h < 21$
	$-12 < k < 11$	$-11 < k < 11$	$0 < k < 20$
	$0 < l < 14$	$0 < l < 31$	$0 < l < 23$
reflns unique	3561	6502	5450
reflns obsd ($\|F_o\| > 4\sigma(F_o)$)	3091	5277	4783
variables	434	632	603
R	0.044	0.048	0.040
ω	$1/(\sigma^2(F_o) + 0.0001(F_o)^2)$	$1/(\sigma^2(F_o) + 0.0001(F_o)^2)$	$1/(\sigma^2(F_o) + 0.0002(F_o)^2)$
R_ω	0.049	0.047	0.045
max Fourier diff, e Å^{-3}	−0.28, 0.20	−0.30, 0.24	−1.18, 0.74

Hz). ^{13}C NMR in $CDCl_3$: δ 14.19, 15.54 (primary C); 22.27, 26.00, 29.15, 29.42, 29.60, 29.70, 31.90, 40.15, 66.30 (secondary C); 110.50, 112.90, 114.33, 132.20, 126.00, 138.00 (tertiary C); 118.70, 121.62, 128.22, 138.42, 147.20, 163.50, 165.70 (quaternary C). ES-MS (CH_2Cl_2): m/z 976.3 ($[M + H]^+$).

Preparation of the Complexes $[La(L^{14})(NO_3)_3]\cdot 3H_2O$ (22), $[Ln(L^{14})(NO_3)_3]\cdot H_2O$ (Ln = Sm, 23; Eu, 24; Gd, 25; Tb, 26; Yb, 27; Lu, 28; Y, 29) and $[Lu(L^{13})(NO_3)_3]\cdot 3CH_3CN$ (30). L^{14} (50 mg, 0.053 mmol) in dichloromethane (5 mL) was added to $Ln(NO_3)_3\cdot xH_2O$ (Ln = La, Sm, Eu, Gd, Yb, Lu, Y; $x = 2-6$, 0.053 mmol) in acetonitrile (5 mL). After 1 h of stirring at room temperature, the solvents were evaporated to dryness, and the residual solid was solubilized in a minimum of hot acetonitrile. Cooling the solution produced white powders, which were again recrystallized from acetonitrile (propionitrile or isobutyronitrile) to give 61−84% of complexes $[Ln(L^{14})(NO_3)_3]\cdot H_2O$ (Ln = Sm, **23**; Eu, **24**; Gd, **25**; Tb, **26**; Yb, **27**; Lu, **28**; Y, **29**). X-ray quality crystals of $[Lu(L^{13})(NO_3)_3]\cdot 3CH_3CN$ (**30**) were obtained with the same procedure using L^{13}. Complexes **22**−**29** were characterized by their IR spectra and gave satisfactory elemental analyses (Table S13 in the Supporting Information).

Physicochemical Measurements. Reflectance spectra were recorded as finely ground powders dispersed in MgO (5%) with MgO as reference on a Perkin-Elmer Lambda 900 spectrophotometer equipped with a PELA-1000 integration sphere from Labsphere. Electronic spectra in the UV−visible range were recorded at 20 °C from $10^{-3}-10^{-4}$ M dichloromethane/acetonitrile solutions with a Perkin-Elmer Lambda 5 spectrometer using quartz cells of 0.1- and 1-cm path length. Spectrophotometric titrations were performed with a Perkin-Elmer Lambda 5 spectrophotometer connected to an external computer. In a typical experiment, 25 mL of ligand L^{14} (10^{-4} M) in dichloromethane/acetonitrile (1:1) was titrated at 20 °C with a solution of $Ln(NO_3)_3\cdot 3H_2O$, 1 mM in acetonitrile. After each addition of 0.1 mL, the absorption spectra were recorded using a 0.1-cm quartz cell and transferred to the computer. Plots of extinction as a function of the metal/ligand ratio gave a first indication of the number and stoichiometry of the complexes formed; factor analysis was then applied to the data to confirm the number of different absorbing species, and finally, a model for the distribution of species was fitted with a nonlinear least-squares algorithm to give stability constants using the SPECFIT program.[45] IR spectra were obtained from KBr pellets with a Perkin-Elmer 883 spectrometer. ^{1}H and ^{13}C NMR spectra were recorded at 25 °C on a Broadband Varian Gemini 300 spectrometer. Chemical shifts are given in ppm with respect to TMS. EI-MS (70 eV) were recorded with VG-7000E and Finnigan-4000 instruments. Pneumatically assisted electrospray (ES-MS) mass spectra were recorded from dichloromethane solutions for the ligands on a Finnigan MAT SSQ 7000 and from 10^{-4} M acetonitrile solution for the complexes on an API III tandem mass spectrometer (PE Sciex). The spectra were recorded under low up-front declustering or collision-induced dissociation (CID) conditions, typically $\Delta V = 0-30$ V between the orifice and the first quadrupole of the spectrometer.[46] The experimental procedures for high-resolution, laser-excited luminescence measurements have been published previously.[14,15] Solid-state samples were finely powdered, and low temperature (77 or 10 K) was achieved by means of a Cryodyne model 22 closed-cycle refrigerator from CTI Cryogenics. Luminescence spectra were corrected for the instrumental function, but not excitation spectra. Lifetimes are averages of at least 3−5 independent determinations. Ligand excitation and emission spectra were recorded on a Perkin-Elmer LS-50B spectrometer equipped for low-temperature measurements. The relative quantum yields were calculated using the following formula:[15] $Q_x/Q_r = \langle A_r(\lambda_r)/A_x(\lambda_x)\rangle\langle I(\lambda_r)/I(\lambda_x)\rangle\langle n^2_x/n^2_r\rangle\langle D_x/D_r\rangle$, where subscript r stands for the reference and x for the samples; A is the absorbance at the excitation wavelength, I is the intensity of the excitation light at the same wavelength, n is the refractive index (1.341 for all solutions in acetonitrile), and D is the measured integrated luminescence intensity. DSC traces were obtained with a Seiko DSC 220C differential scanning calorimeter from 3−5 mg samples (5−10 °C·min^{-1}, under N_2). Thermogravimetric analyses were performed with a thermogravimetric balance Seiko TG/DTA 320 (under N_2). The characterization of the mesophases was performed with a polarizing microscope, Zeiss Axioskop, equipped with a Linkam THMS 600 variable-temperature stage. Powder X-ray diffraction patterns were recorded as a function of temperature using a Debye−Scherrer type camera with bent quartz monochromator (Cu Kα

(45) Gampp, H.; Maeder, M.; Meyer, C. J.; Zuberbühler, A. D. *Talanta* **1985**, *32*, 257.

(46) Hopfgartner, G.; Piguet, C.; Henion, J. D. *J. Am. Soc. Mass Spectrom.* **1994**, *5*, 748.

radiation, $\lambda = 1.5418$ Å), an INSTEC hotstage (±0.01 °C), and an INEL curved position-sensitive gas detector associated with a data acquisition computer system. It was possible to measure periodic distances up to 60 Å, with experimental resolution of $2\theta = 0.07°$. Some of the patterns were also registered photographically using Guinier cameras. Elemental analyses were performed by Dr. H. Eder from the Microchemical Laboratory of the University of Geneva. Metal contents were determined by ICP (Perkin-Elmer Plasma 1000) using internal standard techniques after mineralization of the complexes.

X-ray Crystal Structure Determination of L^{13}, L^{16}, and $[Lu(L^{13})(NO_3)_3]\cdot 3CH_3CN$ (30). A summary of the crystal data, intensity measurements, and structure refinements is reported in Table 8.

(i) Data Collection and Processing. Stoe STADI4 diffractometer, $\omega-2\theta$ scan, scan width $= 1.05 + 0.35 \tan\theta$, scan speed $0.06°\cdot s^{-1}$, Cu Kα radiation ($\lambda = 1.5418$ Å). Two reference reflections were measured every 45 min and showed no significant variations.

(ii) Structure Analysis and Refinement. Data were corrected for Lorentz, polarization, and absorption effects.[47] The structures were solved by direct methods using MULTAN 87;[48] all other calculations used XTAL[49] system and ORTEP II[24] programs. Full-matrix least-squares refinements (on *F*). The non-H atoms were refined with anisotropic displacement parameters, except for the non-H atoms of the disordered solvent molecules in **30**. H atoms were placed in calculated positions and contributed to F_c calculations.

Acknowledgment. We gratefully acknowledge Ms. H. Lartigue and V. Foiret for their technical assistance, Ms. M.-T. Vilches for observation of textures by polarizing microscopy, and Dr. G. Hopfgartner (Hofmann-La Roche) for recording ES-MS spectra of the complexes. C.P. thanks the Werner Foundation for a fellowship, and J.-C.G.B. thanks the Fondation Herbette (Lausanne) for the gift of spectroscopic equipment. This work is supported through grants from the Swiss National Science Foundation.

Supporting Information Available: Tables of atomic coordinates, bond distances and bond angles, anisotropic displacements parameters and selected least-squares planes data for L^{13} (Tables S1−S4), L^{16} (Tables S5−S8), and $[Lu(L^{13})(NO_3)_3](CH_3CN)_3$ (**30**) (Tables S9−S12); Table S13 of elemental analyses for complexes **22**−**29** and Table S14 listing the variable-temperature ^{1}H NMR chemical shifts in $[Y(L^{14})(NO_3)_3]$; Figure F1 showing the emission spectra of $[Tb(L^{14})(NO_3)_3(OH_2)]$ (**26**) measured under excitation through the ligand levels at various temperatures and Figure F2 showing the *d*-layered spacing for L^{14} at different temperatures (29 pages, print/PDF). See any current masthead page for ordering information and Web access instructions.

JA982545N

(47) Blanc, E.; Schwarzenbach, D.; Flack, H. D. *J. Appl. Crystallogr.* **1991**, *24*, 1035.

(48) Main, P.; Fiske, S. J.; Hull, S. E.; Lessinger, L.; Germain, D.; Declercq, J. P.; Woolfson, M. M. *MULTAN 87*; Universities of York, England, and Louvain-La-Neuve, Belgium, 1987.

(49) Hall, S. R., Stewart, J. M., Eds. *XTAL 3.2 User's Manual;* Universities of Western Australia and Maryland, 1992.